

Doubly Constrained Robust Capon Beamformer

Jian Li, *Senior Member, IEEE*, Petre Stoica, *Fellow, IEEE*, and Zhisong Wang, *Student Member, IEEE*

Abstract—The standard Capon beamformer (SCB) is known to have better resolution and much better interference rejection capability than the standard data-independent beamformer when the array steering vector is accurately known. However, the major problem of the SCB is that it lacks robustness in the presence of array steering vector errors. In this paper, we will first provide a complete analysis of a norm constrained Capon beamforming (NCCB) approach, which uses a norm constraint on the weight vector to improve the robustness against array steering vector errors and noise. Our analysis of NCCB is thorough and sheds more light on the choice of the norm constraint than what was commonly known. We also provide a natural extension of the SCB, which has been obtained via covariance matrix fitting, to the case of uncertain steering vectors by enforcing a double constraint on the array steering vector, viz. a constant norm constraint and a spherical uncertainty set constraint, which we refer to as the doubly constrained robust Capon beamformer (DCRCB). NCCB and DCRCB can both be efficiently computed at a comparable cost with that of the SCB. Performance comparisons of NCCB, DCRCB, and several other adaptive beamformers via a number of numerical examples are also presented.

Index Terms—Adaptive arrays, array errors, diagonal loading, doubly restrained robust capon beamforming, robust adaptive beamforming, robust capon beamforming, signal power estimation, steering vector uncertainty set.

I. INTRODUCTION

ARRAY signal processing has wide applications in radar, sonar, acoustics, astronomy, seismology, communications, and medicine. One of the most important tasks of array processing is beamforming. The standard data-independent beamformers include the delay-and-sum approach, which is known to suffer from poor resolution and high sidelobe problems, as well as methods based on various data-independent weight vectors for sidelobe control [1], [2] at the cost of even poorer resolution. The data-dependent Capon beamformer adaptively selects the weight vector to minimize the array output power subject to the linear constraint that the signal of interest (SOI) does not suffer from any distortion [1]–[4]. The Capon beamformer has better resolution and much better interference rejection capability than the data-independent beamformer, provided that the array steering vector corresponding to the SOI is accurately known.

However, the knowledge of the SOI steering vector can be imprecise, which is often the case in practice due to differences between the assumed signal arrival angle and the true arrival angle or between the assumed array response and the true array response (array calibration errors). Whenever this happens, the Capon beamformer may suppress the SOI as an interference, which results in significantly underestimated SOI power and drastically reduced array output signal-to-interference-plus-noise ratio (SINR). Then, the performance of the Capon beamformer may become worse than that of the standard beamformers [5], [6].

The same happens when the number of snapshots is relatively small (i.e., about the same as the number of sensors). In fact, there is a close relationship between the cases of steering vector errors and small-sample errors (see, for example, [7]) in the sense that the difference between the sample covariance matrix $\hat{\mathbf{R}}$ (estimated from a finite number of snapshots) and the corresponding theoretical (ensemble) covariance matrix \mathbf{R} can be viewed as due to steering vector errors.

Many approaches have been proposed during the past three decades to improve the robustness of the Capon beamformer, and the literature on robust adaptive beamforming is extensive (see, for example, [2] and [8]–[12] and the many references therein). Among these robust approaches, diagonal loading (including its extended versions) has been a popular and widely used approach to improve the robustness of the Capon beamformer (see, e.g., [13]–[23] and the references therein for more early suggested methods). However, for most of the diagonal loading methods, it is not clear how to choose the diagonal loading level based on information about the uncertainty of the array steering vector.

Only recently have some methods with a clear theoretical background been proposed (see, for example, [10]–[12] and [24]–[26]) which, unlike the early methods, make explicit use of an uncertainty set of the array steering vector. In [24], a polyhedron is used to describe the uncertainty set, whereas spherical and ellipsoidal (including flat ellipsoidal) uncertainty sets are considered in [10]–[12] and [25]. The robust Capon beamforming approaches presented in [10] and [11] coupled the formulation of the standard Capon beamformer (SCB) in [3] with a spherical or ellipsoidal uncertainty set of the array steering vector, whereas we coupled the formulation of SCB in [27] with an ellipsoidal uncertainty set to obtain a Robust Capon Beamformer (RCB) in [12] and [25]. Interestingly, the methods in [10]–[12] and [25] turn out to be equivalent and to belong to the extended class of diagonal loading approaches, but the corresponding amount of diagonal loading can be calculated precisely based on the ellipsoidal uncertainty set. However, our RCB in [12] is simpler and computationally more efficient than its equivalent counterparts, and its computational complexity is

Manuscript received March 27, 2003; revised September 20, 2003. This work was supported in part by the National Science Foundation under Grants CCR-0104887 and ECS-0097636 and the Swedish Science Council (VR). The associate editor coordinating the review of this manuscript and approving it for publication was Dr. Hamid Krim.

J. Li and Z. Wang are with the Department of Electrical and Computer Engineering, University of Florida, Gainesville, FL 32611 USA (e-mail: li@dsp.ufl.edu).

P. Stoica is with the Department of Systems and Control, Uppsala University, SE-75105 Uppsala, Sweden.

Digital Object Identifier 10.1109/TSP.2004.831998

comparable to that of SCB (see [12] for details). Moreover, our RCB gives a simple way of eliminating the scaling ambiguity when estimating the power of the desired signal, whereas the approaches in [10] and [11] did not consider the scaling ambiguity problem.

In this paper, we will first provide a complete analysis of a norm constrained Capon beamforming (NCCB) approach, which uses a norm constraint on the weight vector to improve the robustness against array steering vector errors and noise. Our analysis is thorough and sheds more light on the choice of the norm constraint than what was previously known [13]. We also provide a natural extension of SCB, which has been obtained via covariance matrix fitting, to the case of uncertain steering vectors by enforcing a double constraint on the steering vector, viz. a constant norm constraint and a spherical uncertainty set constraint, which we refer to as the doubly constrained robust Capon beamformer (DCRCB). We show that the DCRCB algorithm provides an exact solution to the aforementioned constrained optimization problem, which is not convex, whereas the RCB algorithm in [12] and [25] provides an approximate solution by first solving a convex optimization problem without the norm constraint and then imposing the norm constraint by possibly violating the uncertainty set constraint. We also show that like RCB, both NCCB and DCRCB can be efficiently computed at a comparable cost with that of SCB. Additionally, we provide insights into the choice of the smallest spherical uncertainty set for the SOI steering vector. Performance comparisons of NCCB, DCRCB, and RCB via a number of numerical examples are also presented. For the comparison with the eigenspace beamformer, see the numerical examples in [10].

Our paper is organized as follows. In Section II, we formulate the problem of interest. In Section III, we provide a complete analysis of NCCB. In Section IV, we present the DCRCB algorithm and explain its relationship to RCB. We also explain how to choose the smallest spherical uncertainty set for the SOI steering vector. Numerical examples comparing the performance of SCB, NCCB, RCB, and DCRCB are given in Section V. Finally, Section VI presents our conclusions.

II. PROBLEM FORMULATION

Consider an array comprising M sensors, and let \mathbf{R} denote the theoretical covariance matrix of the array output vector. We assume that $\mathbf{R} > 0$ (positive definite) has the following form:

$$\mathbf{R} = \sigma_0^2 \mathbf{a}_0 \mathbf{a}_0^* + \sum_{k=1}^K \sigma_k^2 \mathbf{a}_k \mathbf{a}_k^* + \mathbf{Q} \quad (1)$$

where $(\sigma_0^2, \{\sigma_k^2\}_{k=1}^K)$ are the powers of the $(K+1)$ uncorrelated signals impinging on the array, $(\mathbf{a}_0, \{\mathbf{a}_k\}_{k=1}^K)$ are the so-called steering vectors that depend on the array geometry and are functions of the location parameters of the sources emitting the signals [e.g., their directions-of-arrival (DOAs)], $(\cdot)^*$ denotes the conjugate transpose, and \mathbf{Q} is the noise covariance matrix [the “noise” comprises nondirectional signals, and hence, \mathbf{Q} usually has full rank as opposed to the other terms in (1) whose rank is equal to one]. In what follows, we assume that the first term in

(1) corresponds to the signal-of-interest (SOI) and the remaining rank-one terms to K interferences. To avoid ambiguities, we assume that

$$\|\mathbf{a}_0\|^2 = M \quad (2)$$

where $\|\cdot\|$ denotes the Euclidean norm. We note that the above expression for \mathbf{R} holds for both narrowband and wideband signals; in the former case, \mathbf{R} is the covariance matrix at the carrier frequency, and in the latter case, \mathbf{R} is the covariance matrix at the center of a given frequency bin. In practical applications, \mathbf{R} is replaced by the sample covariance matrix $\hat{\mathbf{R}}$, where

$$\hat{\mathbf{R}} = \frac{1}{N} \sum_{n=1}^N \mathbf{x}_n \mathbf{x}_n^* \quad (3)$$

with N denoting the number of snapshots and \mathbf{x}_n representing the n th snapshot.

The *robust beamforming problem* that we will deal with in this paper can now be briefly stated as follows: Extend the Capon beamformer in order to be able to accurately determine the power of SOI, even when only an imprecise knowledge of its steering vector \mathbf{a}_0 is available. More specifically, we assume that the only knowledge we have about \mathbf{a}_0 is that it belongs to the following uncertainty sphere:

$$\|\mathbf{a}_0 - \bar{\mathbf{a}}\|^2 \leq \epsilon \quad (4)$$

where $\bar{\mathbf{a}}$ and ϵ are given ($\bar{\mathbf{a}}$ is the assumed steering vector of SOI, and ϵ is a user parameter whose choice will be discussed later on). We also assume that the steering vector $\bar{\mathbf{a}}$ satisfies the same norm constraint as \mathbf{a}_0 of (2):

$$\|\bar{\mathbf{a}}\|^2 = M. \quad (5)$$

The assumption that $\|\mathbf{a}_0\|^2 = M$ (we choose $\bar{\mathbf{a}}$) is reasonable for many scenarios including the cases of the look direction error and phase perturbations. It is violated when the array response vector also has gain perturbations. However, if the gain perturbations are small, the norm constraint still holds approximately (as in Section V for the numerical examples).

In this paper, we focus on the problem of estimating the SOI power σ_0^2 from \mathbf{R} (or more practically $\hat{\mathbf{R}}$) when the knowledge of \mathbf{a}_0 is imprecise. However, the beamforming approaches we present herein can also be used for other applications, including signal waveform estimation.

III. NORM CONSTRAINED CAPON BEAMFORMING

The common formulation of the adaptive beamforming problem that leads to SCB, when \mathbf{a}_0 is assumed known, is as follows (see, e.g., [1], [3], [4]):

a) Determine the $M \times 1$ vector \mathbf{w}_0 that is the solution to the following linearly constrained quadratic problem:

$$\min_{\mathbf{w}} \mathbf{w}^* \mathbf{R} \mathbf{w} \quad \text{subject to} \quad \mathbf{w}^* \mathbf{a}_0 = 1. \quad (6)$$

b) Use $\mathbf{w}_0^* \mathbf{R} \mathbf{w}_0$ as an estimate of σ_0^2 .

The solution to (6) is easily derived:

$$\mathbf{w}_0 = \frac{\mathbf{R}^{-1}\mathbf{a}_0}{\mathbf{a}_0^*\mathbf{R}^{-1}\mathbf{a}_0}. \quad (7)$$

Using (7) in Step b) above yields the following estimate of σ_0^2 :

$$\hat{\sigma}_0^2 = \frac{1}{\mathbf{a}_0^*\mathbf{R}^{-1}\mathbf{a}_0}. \quad (8)$$

The SCB adaptively selects the weight vector to minimize the array output power subject to the linear constraint that SOI does not suffer from any distortions [1]–[4]. SCB has better resolution and much better interference rejection capability than data-independent beamformers, provided that \mathbf{a}_0 is accurately known. However, the knowledge of \mathbf{a}_0 can be imprecise, which is often the case in practice due to the differences between the assumed signal arrival angle and the true arrival angle or between the assumed array response and the true array response (array calibration errors). Whenever this happens, we use the assumed $\bar{\mathbf{a}}$ in lieu of the true \mathbf{a}_0 in the SCB, and the performance of SCB may become worse than that of the standard beamformers [5], [6]; specifically, in such a case, SCB may attempt to suppress the SOI as if it were an interference. Since \mathbf{a}_0 is usually close to $\bar{\mathbf{a}}$, the Euclidean norm of the resulting weight vector (which equals the white noise gain at the array output) can become very large in order to satisfy the distortionless constraint $\mathbf{w}^*\bar{\mathbf{a}} = 1$ and at the same time cancels the SOI, i.e., $\mathbf{w}^*\mathbf{a}_0 \approx 0$ (note that the previous two conditions on \mathbf{w} imply $\mathbf{w}^*(\bar{\mathbf{a}} - \mathbf{a}_0) \approx 1$, which can hold only if $\|\mathbf{w}\|^2 \gg 1$ whenever $\|\bar{\mathbf{a}} - \mathbf{a}_0\|^2$ is relatively small).

The goal of NCCB is to impose an additional constraint on the Euclidean norm of \mathbf{w} for the purpose of improving the robustness of the Capon beamformer against SOI steering vector errors and noise (see, e.g., [13]–[17] and the references therein). Consequently, the beamforming problem is formulated as follows:

$$\min_{\mathbf{w}} \mathbf{w}^*\mathbf{R}\mathbf{w} \quad \text{subject to} \quad \mathbf{w}^*\bar{\mathbf{a}} = 1 \\ \|\mathbf{w}\|^2 \leq \zeta. \quad (9)$$

The problem with NCCB is that the choice of ζ is not easy to make. In particular, this choice is not directly linked to the ϵ in (4) or the uncertainty of the SOI steering vector. The DCRCB algorithm that we will present in Section IV, on the other hand, does not suffer from this problem.

A solution to (9) was found in [13] using the Lagrange multiplier methodology. We provide herein a more thorough analysis of the optimization problem in (9), which provides new insights into the choice of ζ and prepares the grounds for solving the DCRCB optimization problem, which will be discussed later on.

Let \mathcal{S} be the set defined by the constraints in (9). In addition, let

$$g_1(\mathbf{w}, \lambda, \mu) = \mathbf{w}^*\mathbf{R}\mathbf{w} + \lambda(\|\mathbf{w}\|^2 - \zeta) + \mu(-\mathbf{w}^*\bar{\mathbf{a}} - \bar{\mathbf{a}}^*\mathbf{w} + 2) \quad (10)$$

where λ and μ are the real-valued Lagrange multipliers with μ being arbitrary and $\lambda \geq 0$ satisfying $\mathbf{R} + \lambda\mathbf{I} > 0$ so that $g_1(\mathbf{w}, \lambda, \mu)$ can be minimized with respect to \mathbf{w} . (This optimization problem is somewhat similar to the one in [28].) Then

$$g_1(\mathbf{w}, \lambda, \mu) \leq \mathbf{w}^*\mathbf{R}\mathbf{w} \quad \text{for any} \quad \mathbf{w} \in \mathcal{S} \quad (11)$$

with equality on the boundary of \mathcal{S} .

Consider the condition

$$\frac{\bar{\mathbf{a}}^*\mathbf{R}^{-2}\bar{\mathbf{a}}}{[\bar{\mathbf{a}}^*\mathbf{R}^{-1}\bar{\mathbf{a}}]^2} \leq \zeta. \quad (12)$$

When the condition in (12) is satisfied, the SCB solution in (7) with \mathbf{a}_0 replaced by $\bar{\mathbf{a}}$, i.e.,

$$\hat{\mathbf{w}} = \frac{\mathbf{R}^{-1}\bar{\mathbf{a}}}{\bar{\mathbf{a}}^*\mathbf{R}^{-1}\bar{\mathbf{a}}} \quad (13)$$

satisfies the norm constraint in (9) and, hence, is also the NCCB solution. For this case, $\lambda = 0$ and the norm constraint in (9) is inactive.

Otherwise, we have the condition

$$\zeta < \frac{\bar{\mathbf{a}}^*\mathbf{R}^{-2}\bar{\mathbf{a}}}{[\bar{\mathbf{a}}^*\mathbf{R}^{-1}\bar{\mathbf{a}}]^2} \quad (14)$$

which is an upper bound on ζ so that NCCB is different from SCB. To deal with this case, we note that (10) can be written as

$$g_1(\mathbf{w}, \lambda, \mu) = [\mathbf{w} - \mu(\mathbf{R} + \lambda\mathbf{I})^{-1}\bar{\mathbf{a}}]^*(\mathbf{R} + \lambda\mathbf{I}) \cdot [\mathbf{w} - \mu(\mathbf{R} + \lambda\mathbf{I})^{-1}\bar{\mathbf{a}}] - \mu^2\bar{\mathbf{a}}^*(\mathbf{R} + \lambda\mathbf{I})^{-1}\bar{\mathbf{a}} - \lambda\zeta + 2\mu. \quad (15)$$

Hence, the *unconstrained* minimizer of $g_1(\mathbf{w}, \lambda, \mu)$, for fixed λ and μ , is given by

$$\hat{\mathbf{w}}_{\lambda, \mu} = \mu(\mathbf{R} + \lambda\mathbf{I})^{-1}\bar{\mathbf{a}}. \quad (16)$$

Clearly, we have

$$g_2(\lambda, \mu) \triangleq g_1(\hat{\mathbf{w}}_{\lambda, \mu}, \lambda, \mu) = -\mu^2\bar{\mathbf{a}}^*(\mathbf{R} + \lambda\mathbf{I})^{-1}\bar{\mathbf{a}} - \lambda\zeta + 2\mu \quad (17)$$

$$\leq \mathbf{w}^*\mathbf{R}\mathbf{w} \quad \text{for any} \quad \mathbf{w} \in \mathcal{S}. \quad (18)$$

The maximization of $g_2(\lambda, \mu)$ with respect to μ gives

$$\hat{\mu} = \frac{1}{\bar{\mathbf{a}}^*(\mathbf{R} + \lambda\mathbf{I})^{-1}\bar{\mathbf{a}}} \quad (19)$$

and

$$g_3(\lambda) \triangleq g_2(\lambda, \hat{\mu}) = -\lambda\zeta + \frac{1}{\bar{\mathbf{a}}^*(\mathbf{R} + \lambda\mathbf{I})^{-1}\bar{\mathbf{a}}}. \quad (20)$$

The maximization of the above function with respect to λ gives

$$\frac{\bar{\mathbf{a}}^*(\mathbf{R} + \hat{\lambda}\mathbf{I})^{-2}\bar{\mathbf{a}}}{[\bar{\mathbf{a}}^*(\mathbf{R} + \hat{\lambda}\mathbf{I})^{-1}\bar{\mathbf{a}}]^2} = \zeta. \quad (21)$$

We show in Appendix A that, under (14), we have a unique solution $\hat{\lambda} > 0$ to (21) (see also [13]) and that the left side of (21) is a monotonically decreasing function of $\hat{\lambda}$ (see also [23]), and hence, $\hat{\lambda}$ can be obtained efficiently via, for example, a Newton's method.

Note that using (19) in (16) yields

$$\hat{\mathbf{w}} = \frac{(\mathbf{R} + \hat{\lambda}\mathbf{I})^{-1}\bar{\mathbf{a}}}{\bar{\mathbf{a}}^*(\mathbf{R} + \hat{\lambda}\mathbf{I})^{-1}\bar{\mathbf{a}}} \quad (22)$$

which satisfies

$$\hat{\mathbf{w}}^*\bar{\mathbf{a}} = 1 \quad (23)$$

and

$$\|\hat{\mathbf{w}}\|^2 = \zeta. \quad (24)$$

Hence, $\hat{\mathbf{w}}$ belongs to the boundary of \mathcal{S} . Therefore, $\hat{\mathbf{w}}$ is our sought solution. Note that $\hat{\mathbf{w}}$ in (22) has the form of a diagonally loaded Capon beamformer.

We now provide some insights into the choice of ζ for NCCB. From the distortionless constraint in (9), we have

$$1 = |\mathbf{w}^*\bar{\mathbf{a}}|^2 \leq \|\mathbf{w}\|^2 \|\bar{\mathbf{a}}\|^2 \leq \zeta M \quad (25)$$

and hence, we get a lower bound on ζ (see also [2]):

$$\zeta \geq \frac{1}{M}. \quad (26)$$

If ζ is less than this lower bound, there is no solution to the NCCB problem. Hence, ζ should be chosen in the interval defined by the inequalities in (14) and (26).

Next, we derive an upper bound on $\hat{\lambda}$. Let

$$\mathbf{R} = \mathbf{U}\mathbf{\Gamma}\mathbf{U}^* \quad (27)$$

where the columns of \mathbf{U} contain the eigenvectors of \mathbf{R} , and the diagonal elements of the diagonal matrix $\mathbf{\Gamma}$, $\gamma_1 \geq \gamma_2 \geq \dots \geq \gamma_M$ are the corresponding eigenvalues. Let

$$\mathbf{z} = \mathbf{U}^*\bar{\mathbf{a}} \quad (28)$$

and let z_m denote the m th element of \mathbf{z} . Then, (21) can be written as (see also [13])

$$\frac{\sum_{m=1}^M \frac{|z_m|^2}{(\gamma_m + \hat{\lambda})^2}}{\left[\sum_{m=1}^M \frac{|z_m|^2}{(\gamma_m + \hat{\lambda})} \right]^2} = \zeta. \quad (29)$$

Hence, we have

$$\zeta \leq \frac{\frac{\|\bar{\mathbf{a}}\|^2}{(\gamma_M + \hat{\lambda})^2}}{\frac{\|\bar{\mathbf{a}}\|^4}{(\gamma_1 + \hat{\lambda})^2}} = \frac{(\gamma_1 + \hat{\lambda})^2}{M(\gamma_M + \hat{\lambda})^2} \quad (30)$$

which gives the following upper bound on $\hat{\lambda}$:

$$\hat{\lambda} \leq \frac{\gamma_1 - (M\zeta)^{1/2}\gamma_M}{(M\zeta)^{1/2} - 1}. \quad (31)$$

We remark that the computations needed by the search for $\hat{\lambda}$ via a Newton's method are negligible compared with those required by the eigendecomposition of the Hermitian matrix \mathbf{R} (or $\hat{\mathbf{R}}$). Hence, the major computational demand of NCCB comes from the eigendecomposition of \mathbf{R} (or $\hat{\mathbf{R}}$), which requires $O(M^3)$ flops. Therefore, the computational complexity of NCCB is comparable with that of the SCB, which also requires $O(M^3)$ flops.

To summarize, NCCB consists of the following steps.

The NCCB Algorithm

- Step 1) Compute the eigendecomposition of \mathbf{R} (or, in practice, of $\hat{\mathbf{R}}$).
- Step 2) If (14) is satisfied, solve (29) for $\hat{\lambda}$, e.g., by a Newton's method, using the knowledge that the solution is unique and it is lower bounded by 0 and upper bounded by (31); otherwise, set $\hat{\lambda} = 0$.
- Step 3) Use the $\hat{\lambda}$ obtained in Step 2 to get

$$\hat{\mathbf{w}} = \frac{\mathbf{U}(\mathbf{\Gamma} + \hat{\lambda}\mathbf{I})^{-1}\mathbf{U}^*\bar{\mathbf{a}}}{\bar{\mathbf{a}}^*\mathbf{U}(\mathbf{\Gamma} + \hat{\lambda}\mathbf{I})^{-1}\mathbf{U}^*\bar{\mathbf{a}}} \quad (32)$$

where the inverse of the diagonal matrix $\mathbf{\Gamma} + \hat{\lambda}\mathbf{I}$ is easily computed, and the vector $\mathbf{z} = \mathbf{U}^*\bar{\mathbf{a}}$ is available from Step 2.

- Step 4) Compute the SOI power estimate of NCCB

$$\hat{\sigma}_0^2 = \frac{\bar{\mathbf{a}}^*\mathbf{U}(\mathbf{\Gamma} + \hat{\lambda}\mathbf{I})^{-2}\mathbf{\Gamma}\mathbf{U}^*\bar{\mathbf{a}}}{[\bar{\mathbf{a}}^*\mathbf{U}(\mathbf{\Gamma} + \hat{\lambda}\mathbf{I})^{-1}\mathbf{U}^*\bar{\mathbf{a}}]^2} \quad (33)$$

(which is obtained using $\hat{\sigma}_0^2 = \hat{\mathbf{w}}^*\mathbf{R}\hat{\mathbf{w}}$).

Consider the case where \mathbf{R} (or $\hat{\mathbf{R}}$) is singular. Let \mathbf{U}_n denote the submatrix of \mathbf{U} containing the eigenvectors corresponding to the zero eigenvalues of \mathbf{R} (or $\hat{\mathbf{R}}$). Then, the upper bound on ζ corresponding to (14) becomes

$$\zeta < \frac{1}{\|\mathbf{U}_n^*\bar{\mathbf{a}}\|^2}. \quad (34)$$

The above condition on ζ prevents the trivial solution that would give $\mathbf{w}^*\mathbf{R}\mathbf{w} = 0$. To see this, observe that $\mathbf{w} = \mathbf{U}_n\mathbf{U}_n^*\bar{\mathbf{a}}/\|\mathbf{U}_n^*\bar{\mathbf{a}}\|^2$ gives $\mathbf{w}^*\mathbf{R}\mathbf{w} = 0$ and also satisfies $\mathbf{w}^*\bar{\mathbf{a}} = 1$; however, under (34), we have $\|\mathbf{w}\|^2 = 1/\|\mathbf{U}_n^*\bar{\mathbf{a}}\|^2 > \zeta$, and hence, the previous \mathbf{w} violates the norm constraint in (9). When the condition in (34) is satisfied, we still have $\hat{\lambda} > 0$ for NCCB. Moreover, in the steps of NCCB, there is no need that $\gamma_m > 0$ for all $m = 1, 2, \dots, M$. Hence, \mathbf{R} (or $\hat{\mathbf{R}}$) can be singular, under (34), and the NCCB is still usable. In particular, this means that we can allow $N < M$ to compute $\hat{\mathbf{R}}$.

IV. DOUBLY CONSTRAINED ROBUST CAPON BEAMFORMING

We first consider below the derivation of DCRCB and then explain its relationship with the RCB algorithm we presented in [12] and [25].

A. DCRCB Algorithm

To derive DCRCB, we use the reformulation of the Capon beamforming problem in [27] (also see [12] and [25]), to which we append the uncertainty set in (4) and the norm constraint in (2). Proceeding in this way, we *directly* obtain a robust estimate of σ_0^2 , without any intermediate calculation of a vector \mathbf{w} :

$$\begin{aligned} \max_{\sigma^2, \mathbf{a}} \quad & \sigma^2 \quad \text{subject to } \mathbf{R} - \sigma^2\mathbf{a}\mathbf{a}^* \geq 0 \\ & \|\mathbf{a} - \bar{\mathbf{a}}\|^2 \leq \epsilon \\ & \|\mathbf{a}\|^2 = M \end{aligned} \quad (35)$$

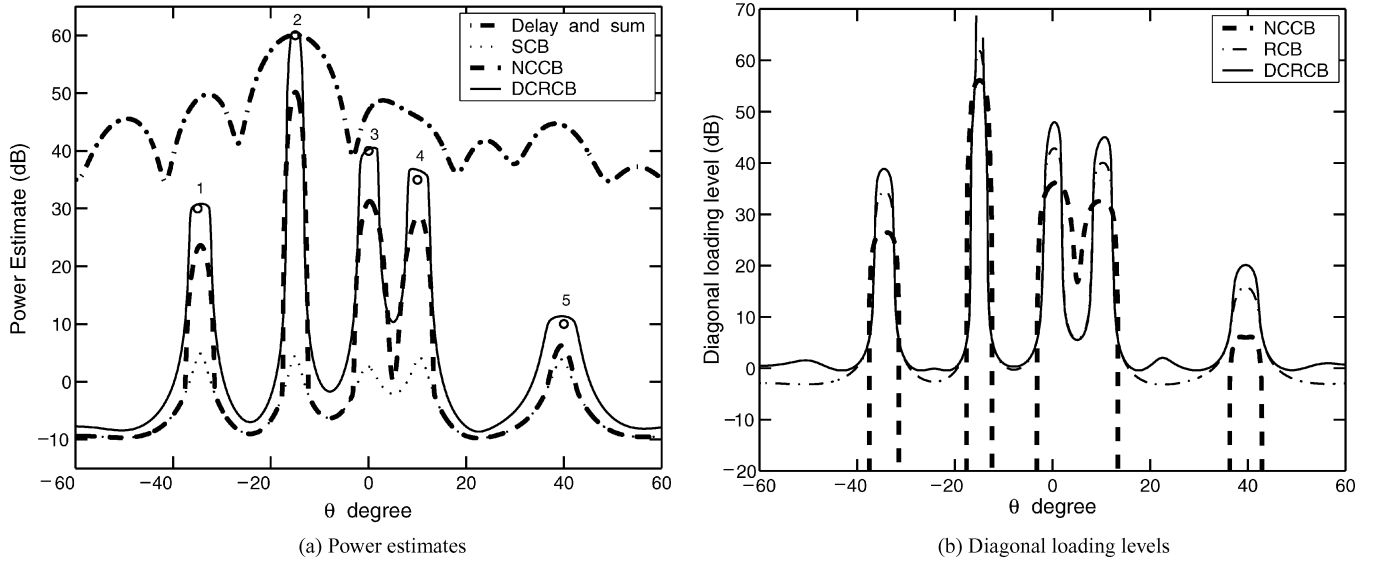


Fig. 1. Power estimates and diagonal loading levels (using \mathbf{R}) versus the steering direction θ when $\epsilon = 1.0$ and $\beta = 6.0$. The true powers of the incident signals from -35° , -15° , 0° , 10° , and 40° are denoted by circles, and $\epsilon_0 = 1.0$.

where $\bar{\mathbf{a}}$ is given and satisfies (5), and ϵ is also given and satisfies $\epsilon > 0$. Note that the first line above can be interpreted as a *covariance fitting problem*: Given \mathbf{R} and \mathbf{a} , we wish to determine the largest possible SOI covariance $\sigma^2 \mathbf{a} \mathbf{a}^*$ that can be a part of \mathbf{R} under the natural constraint that the residual covariance matrix be positive semidefinite; the solution to this problem coincides with the Capon SOI power estimate in (8) (see [25] and [27]).

Using the fact that, for given \mathbf{a} , the solution of (35) w.r.t. σ^2 is obtained by $\sigma_0^2 = 1/(\mathbf{a}^* \mathbf{R}^{-1} \mathbf{a})$ (as mentioned above), the DCRCB problem in (35) can be reduced to the following problem:

$$\min_{\mathbf{a}} \mathbf{a}^* \mathbf{R}^{-1} \mathbf{a} \text{ subject to } \|\mathbf{a} - \bar{\mathbf{a}}\|^2 \leq \epsilon \\ \|\mathbf{a}\|^2 = M. \quad (36)$$

Let $\hat{\mathbf{a}}$ denote the solution to the above optimization problem. The SOI power estimate is then calculated as

$$\hat{\sigma}_0^2 = \frac{1}{\hat{\mathbf{a}}^* \mathbf{R}^{-1} \hat{\mathbf{a}}}. \quad (37)$$

Using $\|\mathbf{a}\|^2 = \|\bar{\mathbf{a}}\|^2 = M$ in (36), we get

$$\min_{\mathbf{a}} \mathbf{a}^* \mathbf{R}^{-1} \mathbf{a} \text{ subject to } \text{Re}(\bar{\mathbf{a}}^* \mathbf{a}) \geq M - \frac{\epsilon}{2} \\ \|\mathbf{a}\|^2 = M. \quad (38)$$

This optimization problem somewhat resembles the NCCB type of problem (see [13]). Consider first the problem (38) without the uncertainty set:

$$\min_{\mathbf{a}} \mathbf{a}^* \mathbf{R}^{-1} \mathbf{a} \text{ subject to } \|\mathbf{a}\|^2 = M. \quad (39)$$

Let \mathbf{u}_1 denote the first eigenvector in \mathbf{U} [see (27)]. The solution $\hat{\mathbf{a}}$ to the above problem is the principal eigenvector \mathbf{u}_1 corresponding to the largest eigenvalue of \mathbf{R} , scaled so that

$$\|\hat{\mathbf{a}}\|^2 = M. \quad (40)$$

As the eigenvector of a matrix is unique only up to a scalar, we can choose the phase of $\hat{\mathbf{a}}$ so that $\text{Re}(\bar{\mathbf{a}}^* \hat{\mathbf{a}})$ is maximum (which is easily done, e.g., $\hat{\mathbf{a}} = M^{1/2} \mathbf{u}_1 e^{j\phi}$, where $\phi = \arg(\mathbf{u}_1^* \bar{\mathbf{a}})$). If the so-obtained $\hat{\mathbf{a}}$ satisfies $\text{Re}(\bar{\mathbf{a}}^* \hat{\mathbf{a}}) \geq M - \epsilon/2$, then it is our sought solution $\hat{\mathbf{a}}$ to (38), and the uncertainty set is an inactive constraint.

If not, i.e., if

$$\text{Re}(\bar{\mathbf{a}}^* \hat{\mathbf{a}}) < M - \frac{\epsilon}{2} \quad (41)$$

then $\hat{\mathbf{a}}$ is not our sought solution. For this case to occur, ϵ must satisfy

$$\epsilon < 2M - 2\text{Re}(\bar{\mathbf{a}}^* \hat{\mathbf{a}}) \leq 2M \quad (42)$$

where the second inequality above is due to $\text{Re}(\bar{\mathbf{a}}^* \hat{\mathbf{a}}) \geq 0$. Let $\tilde{\mathcal{S}}$ be the set defined by the constraints in (38). To determine the solution to (38) under (41), consider the function:

$$f_1(\mathbf{a}, \check{\lambda}, \check{\mu}) = \mathbf{a}^* \mathbf{R}^{-1} \mathbf{a} + \check{\lambda} (\|\mathbf{a}\|^2 - M) + \check{\mu} (2M - \epsilon - \bar{\mathbf{a}}^* \mathbf{a} - \mathbf{a}^* \bar{\mathbf{a}}) \quad (43)$$

where $\check{\lambda}$ and $\check{\mu}$ are the real-valued Lagrange multipliers with $\check{\mu} \geq 0$ and $\check{\lambda}$ satisfying $\mathbf{R}^{-1} + \check{\lambda} \mathbf{I} > 0$ so that the above function can be minimized with respect to \mathbf{a} . Evidently, we have $f_1(\mathbf{a}, \check{\lambda}, \check{\mu}) \leq \mathbf{a}^* \mathbf{R}^{-1} \mathbf{a}$ for any $\mathbf{a} \in \tilde{\mathcal{S}}$ with equality on the boundary of $\tilde{\mathcal{S}}$. Equation (43) can be written as

$$f_1(\mathbf{a}, \check{\lambda}, \check{\mu}) = [\mathbf{a} - \check{\mu}(\mathbf{R}^{-1} + \check{\lambda} \mathbf{I})^{-1} \bar{\mathbf{a}}]^* (\mathbf{R}^{-1} + \check{\lambda} \mathbf{I}) [\mathbf{a} - \check{\mu}(\mathbf{R}^{-1} + \check{\lambda} \mathbf{I})^{-1} \bar{\mathbf{a}}] - \check{\mu}^2 \bar{\mathbf{a}}^* (\mathbf{R}^{-1} + \check{\lambda} \mathbf{I})^{-1} \bar{\mathbf{a}} - \check{\lambda} M + \check{\mu} (2M - \epsilon). \quad (44)$$

Hence, the *unconstrained* minimization of $f_1(\mathbf{a}, \check{\lambda}, \check{\mu})$ w.r.t. \mathbf{a} , for fixed $\check{\lambda}$ and $\check{\mu}$, is given by

$$\check{\mathbf{a}}_{\check{\lambda}, \check{\mu}} = \check{\mu} (\mathbf{R}^{-1} + \check{\lambda} \mathbf{I})^{-1} \bar{\mathbf{a}}. \quad (45)$$

Clearly, we have

$$f_2(\check{\lambda}, \check{\mu}) \triangleq f_1(\check{\mathbf{a}}_{\check{\lambda}, \check{\mu}}, \check{\lambda}, \check{\mu}) = -\check{\mu}^2 \bar{\mathbf{a}}^* (\mathbf{R}^{-1} + \check{\lambda} \mathbf{I})^{-1} \bar{\mathbf{a}} - \check{\lambda} M + \check{\mu} (2M - \epsilon) \quad (46)$$

$$\leq \mathbf{a}^* \mathbf{R}^{-1} \mathbf{a} \text{ for any } \mathbf{a} \in \tilde{\mathcal{S}}. \quad (47)$$

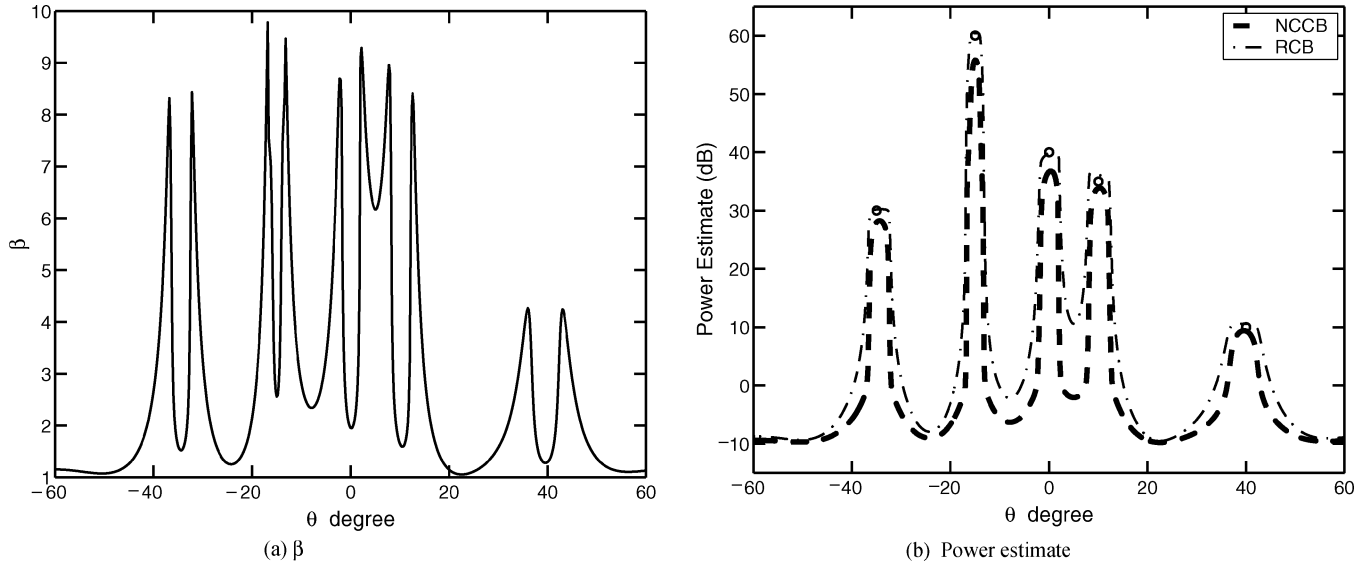


Fig. 2. (a) For each steering direction θ , β is chosen to make NCCB have the same diagonal loading levels as RCB with $\epsilon = 1.0$. (b) Power estimates versus the steering direction θ via the RCB and NCCB approaches. For RCB, $\epsilon = 1.0$. For NCCB, β is chosen as in (a). The true powers of the incident signals from -35° , -15° , 0° , 10° , and 40° are denoted by circles, and $\epsilon_0 = 1.0$.

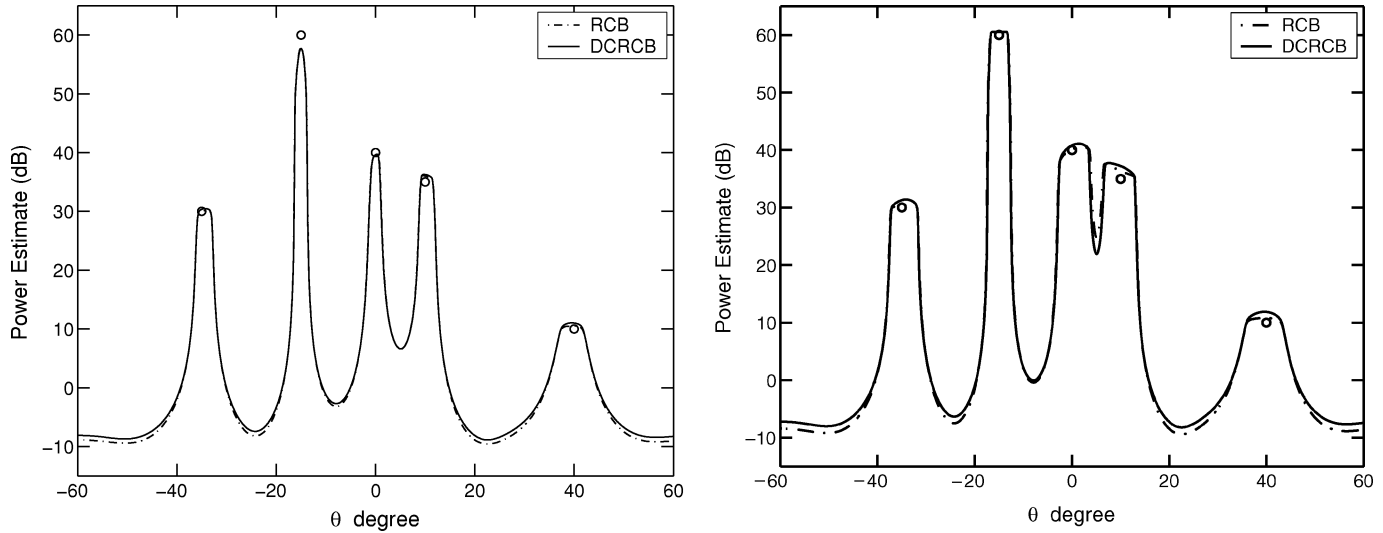


Fig. 3. Power estimates versus the steering direction θ when (a) $\epsilon = 0.7$ and (b) $\epsilon = 1.5$. The true powers of the incident signals from -35° , -15° , 0° , 10° , and 40° are denoted by circles, and $\epsilon_0 = 1.0$.

Maximization of $f_2(\check{\lambda}, \check{\mu})$ with respect to $\check{\mu}$ gives

$$\hat{\mu} = \frac{2M - \epsilon}{2\bar{\mathbf{a}}^*(\mathbf{R}^{-1} + \check{\lambda}\mathbf{I})^{-1}\bar{\mathbf{a}}} \quad (48)$$

which indeed satisfies $\hat{\mu} > 0$ [see (42)]. Inserting (48) into (46), we obtain

$$f_3(\check{\lambda}) \triangleq f_2(\check{\lambda}, \hat{\mu}) = -\check{\lambda}M + \frac{(M - \frac{\epsilon}{2})^2}{\bar{\mathbf{a}}^*(\mathbf{R}^{-1} + \check{\lambda}\mathbf{I})^{-1}\bar{\mathbf{a}}}. \quad (49)$$

Maximization of the above function with respect to $\check{\lambda}$ gives

$$\check{h}(\hat{\lambda}) = \rho \quad (50)$$

where

$$\check{h}(\hat{\lambda}) = \frac{\bar{\mathbf{a}}^*(\mathbf{R}^{-1} + \hat{\lambda}\mathbf{I})^{-2}\bar{\mathbf{a}}}{[\bar{\mathbf{a}}^*(\mathbf{R}^{-1} + \hat{\lambda}\mathbf{I})^{-1}\bar{\mathbf{a}}]^2} \quad (51)$$

and

$$\rho = \frac{M}{(M - \frac{\epsilon}{2})^2}. \quad (52)$$

Similarly to the proof in Appendix A, we can show that, under (41), $\check{h}(\hat{\lambda})$ is a monotonically decreasing function of $\hat{\lambda}$. Moreover, as $\hat{\lambda} \rightarrow \infty$, $\check{h}(\hat{\lambda}) \rightarrow 1/M < \rho$ since $\epsilon > 0$. Furthermore, as $\hat{\lambda} \rightarrow -1/\gamma_1$, $\check{h}(\hat{\lambda}) \rightarrow 1/|\mathbf{u}_1^*\bar{\mathbf{a}}|^2$. Since $|\mathbf{u}_1^*\bar{\mathbf{a}}|^2 = \text{Re}^2(\bar{\mathbf{a}}^*\bar{\mathbf{a}})/M < (M - \epsilon/2)^2/M$ [see (41)], it follows that $1/|\mathbf{u}_1^*\bar{\mathbf{a}}|^2 > \rho$. Hence, there is a unique solution $\hat{\lambda} > -1/\gamma_1$ to (50), which can be obtained efficiently via, for example, a Newton's method. Using (48) in (45) yields

$$\hat{\mathbf{a}} = \left(M - \frac{\epsilon}{2}\right) \frac{(\mathbf{R}^{-1} + \hat{\lambda}\mathbf{I})^{-1}\bar{\mathbf{a}}}{\bar{\mathbf{a}}^*(\mathbf{R}^{-1} + \hat{\lambda}\mathbf{I})^{-1}\bar{\mathbf{a}}} \quad (53)$$

which satisfies

$$\text{Re}(\hat{\mathbf{a}}^* \bar{\mathbf{a}}) = \hat{\mathbf{a}}^* \bar{\mathbf{a}} = M - \frac{\epsilon}{2} \quad (54)$$

and

$$\|\hat{\mathbf{a}}\|^2 = M. \quad (55)$$

Hence, $\hat{\mathbf{a}}$ belongs to the boundary of $\check{\mathcal{S}}$. Therefore, $\hat{\mathbf{a}}$ is the sought solution.

To derive an upper bound on $\hat{\lambda}$, rewrite (50) as

$$\frac{\sum_{m=1}^M \frac{|z_m|^2}{\left(\frac{1}{\gamma_m} + \hat{\lambda}\right)^2}}{\left[\sum_{m=1}^M \frac{|z_m|^2}{\left(\frac{1}{\gamma_m} + \hat{\lambda}\right)}\right]^2} = \rho. \quad (56)$$

Hence, we have

$$\rho \leq \frac{\frac{\|\bar{\mathbf{a}}\|^2}{\left(\frac{1}{\gamma_1} + \hat{\lambda}\right)^2}}{\frac{\|\bar{\mathbf{a}}\|^4}{\left(\frac{1}{\gamma_M} + \hat{\lambda}\right)^2}} = \frac{\left(\frac{1}{\gamma_M} + \hat{\lambda}\right)^2}{M \left(\frac{1}{\gamma_1} + \hat{\lambda}\right)^2} \quad (57)$$

which gives the following upper bound on $\hat{\lambda}$:

$$\hat{\lambda} \leq \frac{\frac{1}{\gamma_M} - (M\rho)^{1/2} \left(\frac{1}{\gamma_1}\right)}{(M\rho)^{1/2} - 1}. \quad (58)$$

To summarize, DCRCB consists of the following steps.

The DCRCB Algorithm

- Step 1) Compute the eigendecomposition of \mathbf{R} (or, more practically, of $\hat{\mathbf{R}}$).
- Step 2) If (41) is satisfied, solve (56) for $\hat{\lambda}$, e.g., by a Newton's method, using the knowledge that the solution is unique and it is lower bounded by $-1/\gamma_1$ and upper bounded by (58), and then continue to Step 3; otherwise, compute $\hat{\sigma}_0^2 = \gamma_1/M$ [which is obtained by using $\hat{\mathbf{a}} = \bar{\mathbf{a}}$ in (37)], and stop.
- Step 3) Use the $\hat{\lambda}$ obtained in Step 2 to get

$$\hat{\mathbf{a}} = \left(M - \frac{\epsilon}{2}\right) \frac{\mathbf{U}(\mathbf{I} + \hat{\lambda}\mathbf{\Gamma})^{-1}\mathbf{\Gamma}\mathbf{U}^*\bar{\mathbf{a}}}{\bar{\mathbf{a}}^*\mathbf{U}(\mathbf{I} + \hat{\lambda}\mathbf{\Gamma})^{-1}\mathbf{\Gamma}\mathbf{U}^*\bar{\mathbf{a}}} \quad (59)$$

where the inverse of the diagonal matrix $\mathbf{I} + \hat{\lambda}\mathbf{\Gamma}$ is easily computed, and $\mathbf{z} = \mathbf{U}^*\bar{\mathbf{a}}$ is available from Step 2.

- Step 4) Compute the SOI power estimate of DCRCB using

$$\hat{\sigma}_0^2 = \frac{1}{\left(M - \frac{\epsilon}{2}\right)^2} \frac{\left[\bar{\mathbf{a}}^*\mathbf{U}(\mathbf{I} + \hat{\lambda}\mathbf{\Gamma})^{-1}\mathbf{\Gamma}\mathbf{U}^*\bar{\mathbf{a}}\right]^2}{\bar{\mathbf{a}}^*\mathbf{U}(\mathbf{I} + \hat{\lambda}\mathbf{\Gamma})^{-2}\mathbf{\Gamma}\mathbf{U}^*\bar{\mathbf{a}}}. \quad (60)$$

Note that the steps above of DCRCB do not require that $\gamma_m > 0$ for all $m = 1, 2, \dots, M$. Hence, \mathbf{R} (or $\hat{\mathbf{R}}$) can also be singular in the DCRCB, which means that we can allow $N < M$ to compute $\hat{\mathbf{R}}$.

We also note that, like for NCCB, the major computational demand of DCRCB comes from the eigendecomposition of \mathbf{R} (or $\hat{\mathbf{R}}$). Therefore, the computational complexity of DCRCB is

also comparable to that of SCB. Moreover, like RCB, DCRCB can be modified for recursive implementation. By using the recursive eigen-decomposition updating, we can update the power and waveform estimates with $O(M^2)$ flops (see [12] and the references therein).

In many applications, such as in communications or the global positioning system, the focus is on SOI waveform estimation. Let $s_0(n)$ denote the waveform of the SOI. Then, once we have estimated the SOI steering vector with DCRCB, $s_0(n)$ can be estimated like in the SCB as follows:

$$\hat{s}_0(n) = \check{\mathbf{w}}^* \mathbf{x}_n \quad (61)$$

where $\hat{\mathbf{a}}$ in (53) is in lieu of \mathbf{a}_0 in (7) to obtain $\check{\mathbf{w}}$:

$$\check{\mathbf{w}} = \frac{\mathbf{R}^{-1}\hat{\mathbf{a}}}{\hat{\mathbf{a}}^*\mathbf{R}^{-1}\hat{\mathbf{a}}} \quad (62)$$

$$= \frac{1}{M - \frac{\epsilon}{2}} \left[\bar{\mathbf{a}}^* \left(\mathbf{R} + \frac{1}{\hat{\lambda}} \mathbf{I} \right)^{-1} \mathbf{R} \bar{\mathbf{a}} \right] \cdot \frac{\left(\mathbf{R} + \frac{1}{\hat{\lambda}} \mathbf{I} \right)^{-1} \bar{\mathbf{a}}}{\bar{\mathbf{a}}^* \left(\mathbf{R} + \frac{1}{\hat{\lambda}} \mathbf{I} \right)^{-1} \mathbf{R} \left(\mathbf{R} + \frac{1}{\hat{\lambda}} \mathbf{I} \right)^{-1} \bar{\mathbf{a}}}. \quad (63)$$

Note that the DCRCB weight vector also has the form associated with the diagonal loading approach, except for the real-valued scaling factor in (63) as well as the fact that the diagonal loading level in (63) can be negative. However, the scaling factor is not really important since the quality of the SOI waveform estimate is typically measured by the signal-to-interference-plus-noise ratio (SINR)

$$\text{SINR} = \frac{\sigma_0^2 |\check{\mathbf{w}}^* \mathbf{a}_0|^2}{\check{\mathbf{w}}^* \left(\sum_{k=1}^K \sigma_k^2 \mathbf{a}_k \mathbf{a}_k^* + \mathbf{Q} \right) \check{\mathbf{w}}} \quad (64)$$

which is independent of the scaling of the weight vector.

B. RCB Algorithm

To make this paper self contained, we also briefly discuss the RCB algorithm presented in [12] and [25] and explain its relationship with the DCRCB algorithm devised in the previous subsection.

Due to the constant norm constraint on \mathbf{a} , the constraint set in (35) is not convex. The problem (35) without the norm constraint on \mathbf{a} is convex. The RCB algorithm obtains an approximate solution to (35) by first finding a solution to the easier convex problem in (35) without the norm constraint on \mathbf{a} and subsequently imposing the norm constraint on the solution by possibly violating the other constraint in (35). More specifically, RCB is derived by first solving the following optimization problem:

$$\min_{\mathbf{a}} \mathbf{a}^* \mathbf{R}^{-1} \mathbf{a} \quad \text{subject to} \quad \|\mathbf{a} - \bar{\mathbf{a}}\|^2 \leq \epsilon. \quad (65)$$

The solution $\check{\mathbf{a}}$ to the above optimization problem can also be determined by using the Lagrange multiplier method, and it has the form (see [12] and [25] for details):

$$\check{\mathbf{a}} = \check{\lambda} \left(\mathbf{R}^{-1} + \check{\lambda} \mathbf{I} \right)^{-1} \bar{\mathbf{a}} \quad (66)$$

where $\check{\lambda} \geq 0$ is the Lagrange multiplier that can be obtained via a Newton's method as the unique solution to the equation

$$\left\| \left(\mathbf{I} + \check{\lambda} \mathbf{R} \right)^{-1} \bar{\mathbf{a}} \right\|^2 = \epsilon. \quad (67)$$

After $\check{\lambda}$ has been obtained, the norm constraint $\|\check{\mathbf{a}}\|^2 = M$ is imposed when estimating the SOI power

$$\hat{\sigma}_0^2 = \frac{\|\check{\mathbf{a}}\|^2}{M \bar{\mathbf{a}}^* \mathbf{R}^{-1} \bar{\mathbf{a}}} \quad (68)$$

$$= \frac{\bar{\mathbf{a}}^* \mathbf{U} (\mathbf{I} + \check{\lambda} \mathbf{R})^{-2} \mathbf{U}^* \bar{\mathbf{a}}}{M \bar{\mathbf{a}}^* \mathbf{U} (\mathbf{I} + \check{\lambda} \mathbf{R})^{-2} \mathbf{U}^* \bar{\mathbf{a}}}. \quad (69)$$

Note that RCB also allows \mathbf{R} (or $\hat{\mathbf{R}}$) to be singular, and it also requires $O(M^3)$ flops for implementation. For SOI waveform estimation, the RCB weight vector has the form

$$\check{\mathbf{w}} = \frac{\left(\mathbf{R} + \frac{1}{\check{\lambda}} \mathbf{I} \right)^{-1} \bar{\mathbf{a}}}{\bar{\mathbf{a}}^* \left(\mathbf{R} + \frac{1}{\check{\lambda}} \mathbf{I} \right)^{-1} \mathbf{R} \left(\mathbf{R} + \frac{1}{\check{\lambda}} \mathbf{I} \right)^{-1} \bar{\mathbf{a}}}. \quad (70)$$

Comparing the $\hat{\mathbf{a}}$ in (53) and $\check{\mathbf{w}}$ in (63) with the $\check{\mathbf{a}}$ in (66) and $\check{\mathbf{w}}$ in (70), we note that, aside from some real-valued scalar factors, the main difference between RCB and DCRCB is in the diagonal loading levels $\check{\lambda}$ for the former and $\hat{\lambda}$ for the latter. The latter diagonal loading level can be negative, whereas the former cannot.

Even though RCB is an approximate solution to (35), it has been shown to have excellent performance [12], [25]. Moreover, in the case of RCB, the spherical uncertainty set in (35) can be readily generalized to both nondegenerate and flat ellipsoidal uncertainty sets. However, it appears that DCRCB is not as easy to generalize to the case of ellipsoidal uncertainty sets as such a generalization would require a two-dimensional search to determine the Lagrange multipliers $\hat{\lambda}$ and $\hat{\mu}$.

C. Smallest Possible Spherical Uncertainty Set

For both RCB and DCRCB, the choice of ϵ should be made as small as possible since when ϵ is chosen too large, the ability of both RCB and DCRCB to suppress interferences that are close to the SOI will degrade. Toward this end, we note that an extra phase on \mathbf{a} will not change the cost function $\mathbf{a}^* \mathbf{R}^{-1} \mathbf{a}$ or the norm constraint $\|\mathbf{a}\|^2 = M$. Hence, ϵ should be chosen as small as possible but such that

$$\epsilon \geq \min_{\alpha} \|\tilde{\mathbf{a}}_0 e^{j\alpha} - \bar{\mathbf{a}}\|^2 \quad (71)$$

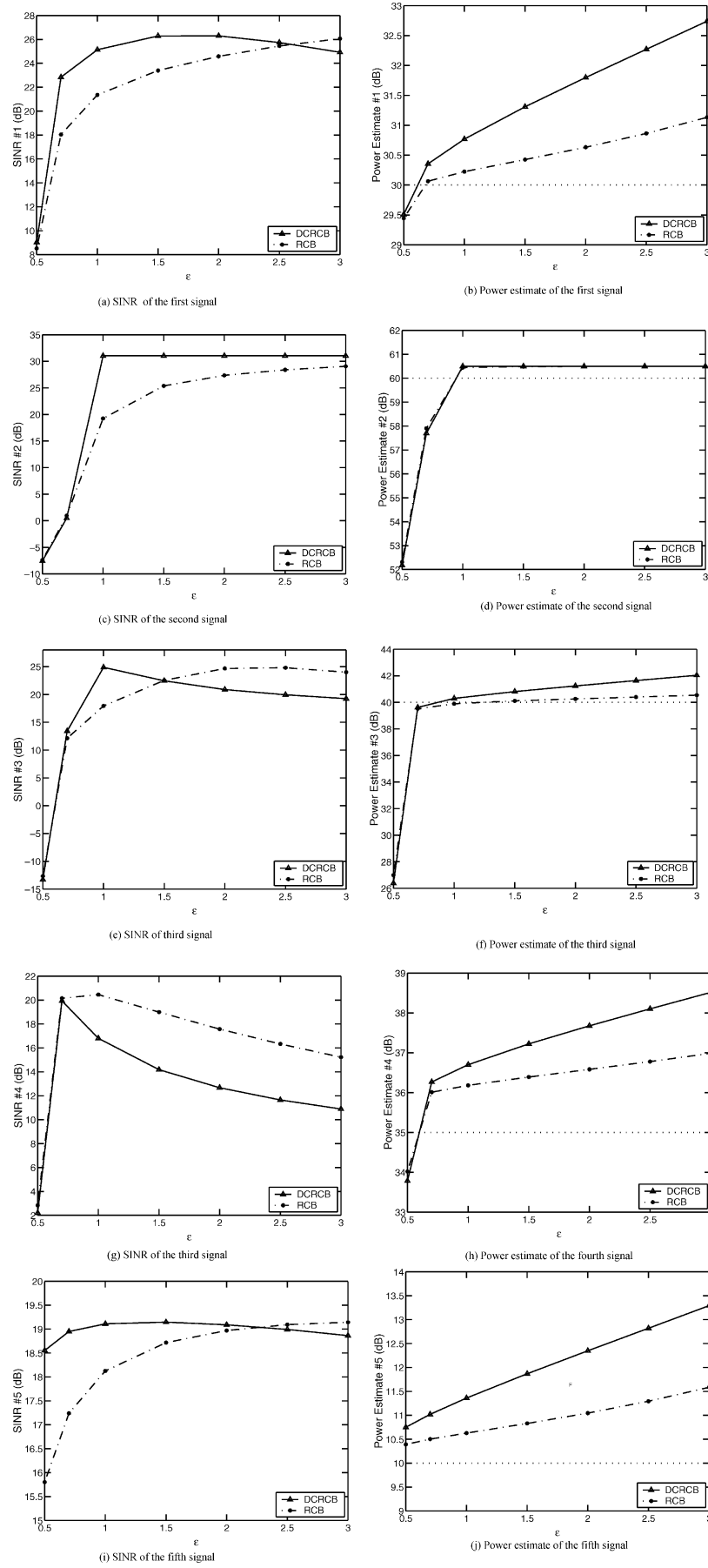
for all possible SOI steering vectors $\tilde{\mathbf{a}}_0$ associated with the true SOI steering vector \mathbf{a}_0 . This analysis explains why it was observed in [12] and [25] that RCB can work well even when $\epsilon < \|\mathbf{a}_0 - \bar{\mathbf{a}}\|^2$. We note that although a phase error in the estimate $\hat{\mathbf{a}}$ or $\check{\mathbf{a}}$ will not affect the SOI power estimate or the array output SINR, the SOI waveform estimate will contain a phase error. In applications such as communications, a training sequence can be used to estimate the phase error and then compensate it out.

V. NUMERICAL EXAMPLES

We provide numerical examples in this section to compare the performances of the delay-and-sum beamformer, SCB, NCCB, RCB, and DCRCB. In all of the examples considered below, we assume a uniform linear array with $M = 10$ sensors and half-wavelength sensor spacing and a spatially white Gaussian noise whose covariance matrix is given by $\mathbf{Q} = \mathbf{I}$. For NCCB, we set $\zeta = \beta/M$, where β ($\beta \geq 1$) is a user parameter. The larger the β , the closer NCCB is to SCB. On the other hand, the smaller the β , the closer NCCB is to the delay-and-sum beamformer. When $\beta = 1$, NCCB becomes the delay-and-sum beamformer, and hence, it uses the assumed array steering vector divided by M as the weight vector. We define the true steering vector error $\epsilon_0 = \min_{\alpha} \|\mathbf{a}_0 e^{j\alpha} - \bar{\mathbf{a}}\|^2$, where \mathbf{a}_0 is the true steering vector, and $\bar{\mathbf{a}}$ is the assumed one. Unless otherwise stated, we use the beamforming methods with the theoretical array covariance matrix \mathbf{R} .

First, we consider an imaging example where we wish to determine the incident signal power as a function of the signal arrival angle θ relative to the array normal. We assume that there are five incident signals with powers 30, 60, 40, 35, and 10 dB from directions -35° , -15° , 0° , 10° , and 40° , respectively. To simulate the array calibration error (the sensor amplitude and phase error as well as the sensor position error), each element of the steering vector for each incident signal is perturbed with a zero-mean circularly symmetric complex Gaussian random variable normalized so that $\epsilon_0 = 1.0$. The perturbing Gaussian random variables are independent of each other. For RCB and DCRCB, we use $\epsilon = 1.0$. For NCCB, we choose $\beta = 6.0$ so that the peak widths of the NCCB and DCRCB are about the same. Fig. 1(a) shows the signal power estimates as functions of the arrival angle θ obtained by using the delay-and-sum beamformer, SCB, NCCB, and DCRCB methods. The small circles in the figure denote the true (direction of arrival, power)-coordinates of the five incident signals. Since the power estimates of RCB and DCRCB are almost the same for this example, only the DCRCB power estimates are shown in the figure. Note that SCB can give good direction-of-arrival estimates for the incident signals based on the peak locations. However, the SCB estimates of the incident signal powers are way off. NCCB is more robust than SCB but still substantially underestimates the signal powers. On the other hand, our DCRCB provides excellent power estimates of the incident sources. As expected, the delay-and-sum beamformer has poorer resolution than the other beamformers. Moreover, the sidelobes of the former result in false peaks. Fig. 1(b) shows the diagonal loading levels of the NCCB, RCB, and DCRCB approaches. Depending on whether the condition of (14) is satisfied or not, NCCB can have a nonzero or zero diagonal loading level. This results in the discontinuities in the NCCB diagonal loading level curve. The discontinuity in the DCRCB diagonal loading level curve is due to the fact that around the strongest signal, the condition of (41) is not satisfied. As a result, DCRCB is no longer a diagonal loading approach around the strongest signal.

For each steering angle θ in Fig. 2(a), β is chosen to make NCCB have the same diagonal loading level as RCB when $\epsilon = 1.0$ is used in RCB. We note that for NCCB and RCB to have


 Fig. 4. Comparison of the RCB and DCRCB approaches for each incident signal, as ϵ varies, when $\epsilon_0 = 1.0$.

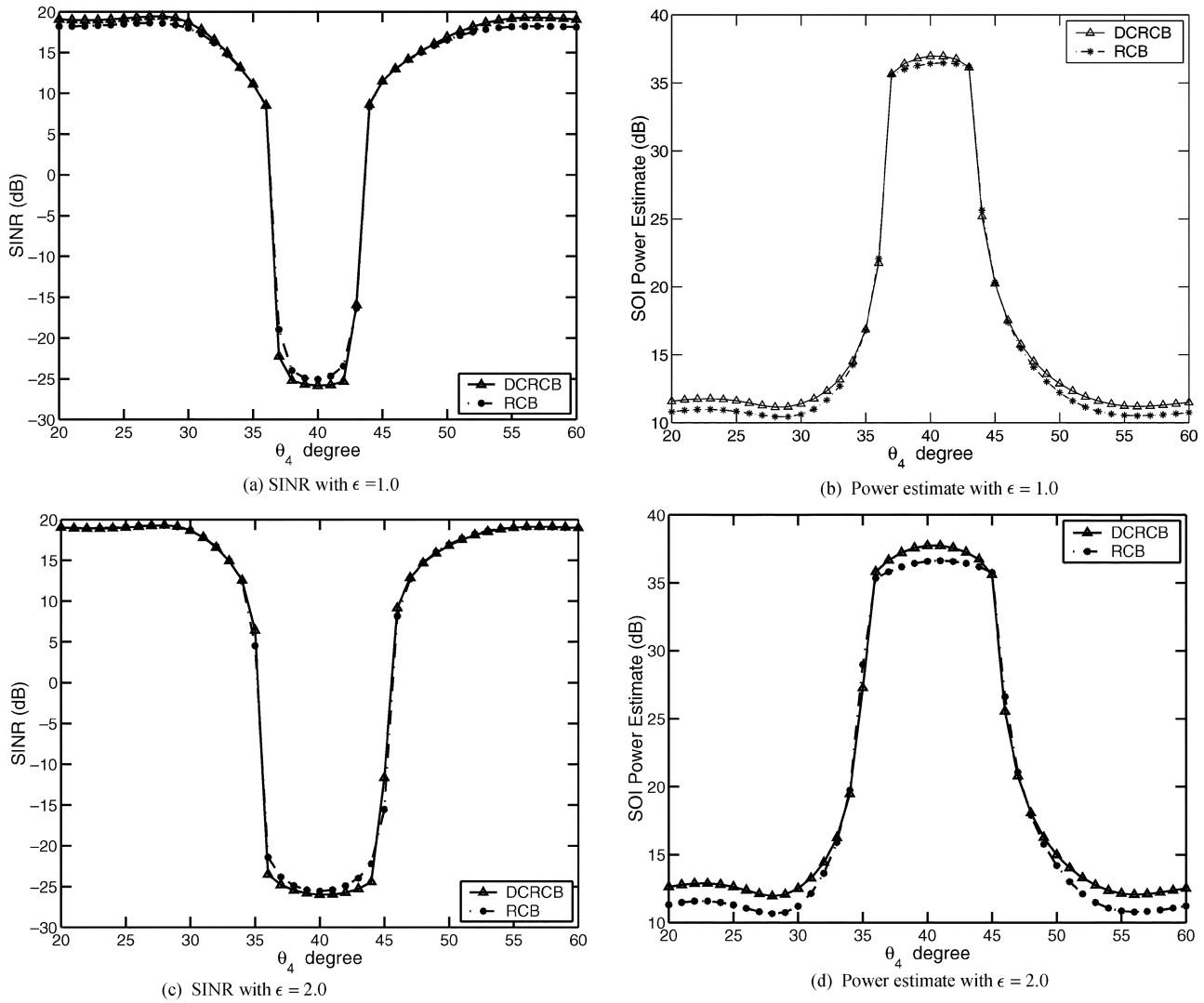


Fig. 5. Comparison of the RCB and DCRCB approaches with (a), (b) $\epsilon = 1.0$ and (c), (d) $\epsilon = 2.0$ when θ_4 (the direction of arrival of the fourth signal) is changing from 20° to 60° . The SOI power is 10 dB, and $\epsilon_0 = 1.0$.

the same diagonal level, β must be chosen in a complicated manner depending on both ϵ and the data itself. Fig. 2(b) shows the signal power estimates as functions of θ obtained via using NCCB and RCB with the β in NCCB chosen so that NCCB and RCB have the same diagonal loading levels. We note that the RCB signal power estimates are much more accurate than those obtained using NCCB, and hence, the norm constraint imposed on $\tilde{\mathbf{a}}$ in (68) is very helpful for accurate SOI power estimation.

Fig. 3(a) and (b) show the power estimates as functions of θ obtained via using RCB and DCRCB with $\epsilon = 0.7$ and $\epsilon = 1.5$, respectively, for the example in Fig. 1. Note that when $\epsilon < \epsilon_0 = 1.0$, the RCB and DCRCB signal power estimates are not as accurate as when $\epsilon > \epsilon_0$, but the peaks are sharper.

In Fig. 4, we compare the SINRs and the signal power estimates for the five incident signals, as functions of ϵ , obtained via using RCB and DCRCB. Fig. 4(a), (c), (e), (g), and (i) show the SINRs of the five signals as functions of ϵ . Fig. 4(b), (d), (f), (h), and (j) show the power estimates of the five signals as functions of ϵ , with the horizontal dotted lines denoting the true signal powers. Note that except for the fourth signal, the SINR of

DCRCB is in general higher than that of RCB when ϵ is not too far from ϵ_0 . Hence, for applications requiring waveform estimation, the former may be preferred over the latter if ϵ_0 is known reasonably accurately. For the second signal in Fig. 4(c), the condition of (41) is not satisfied, and hence, DCRCB uses the scaled principal eigenvector as the estimated steering vector. For this case, DCRCB is always better than RCB, no matter how ϵ is chosen. On the other hand, for signal power estimation, RCB in general outperforms DCRCB and hence may be preferred in applications such as acoustic imaging, where only the signal power distribution as a function of angle or location is of interest. We also note that the larger the ϵ , the more RCB and DCRCB will overestimate the signal power. Therefore, if possible, ϵ should not be chosen much larger than ϵ_0 .

In the next examples, we concentrate on the fifth signal from 40° , which is treated as the signal of interest (SOI). The other four signals are considered to be interferences. In the following figures for the SOI power estimates, the dotted lines correspond to the true SOI power.

First, we consider a scenario where the fourth signal changes its direction of arrival from 20° to 60° with the directions of

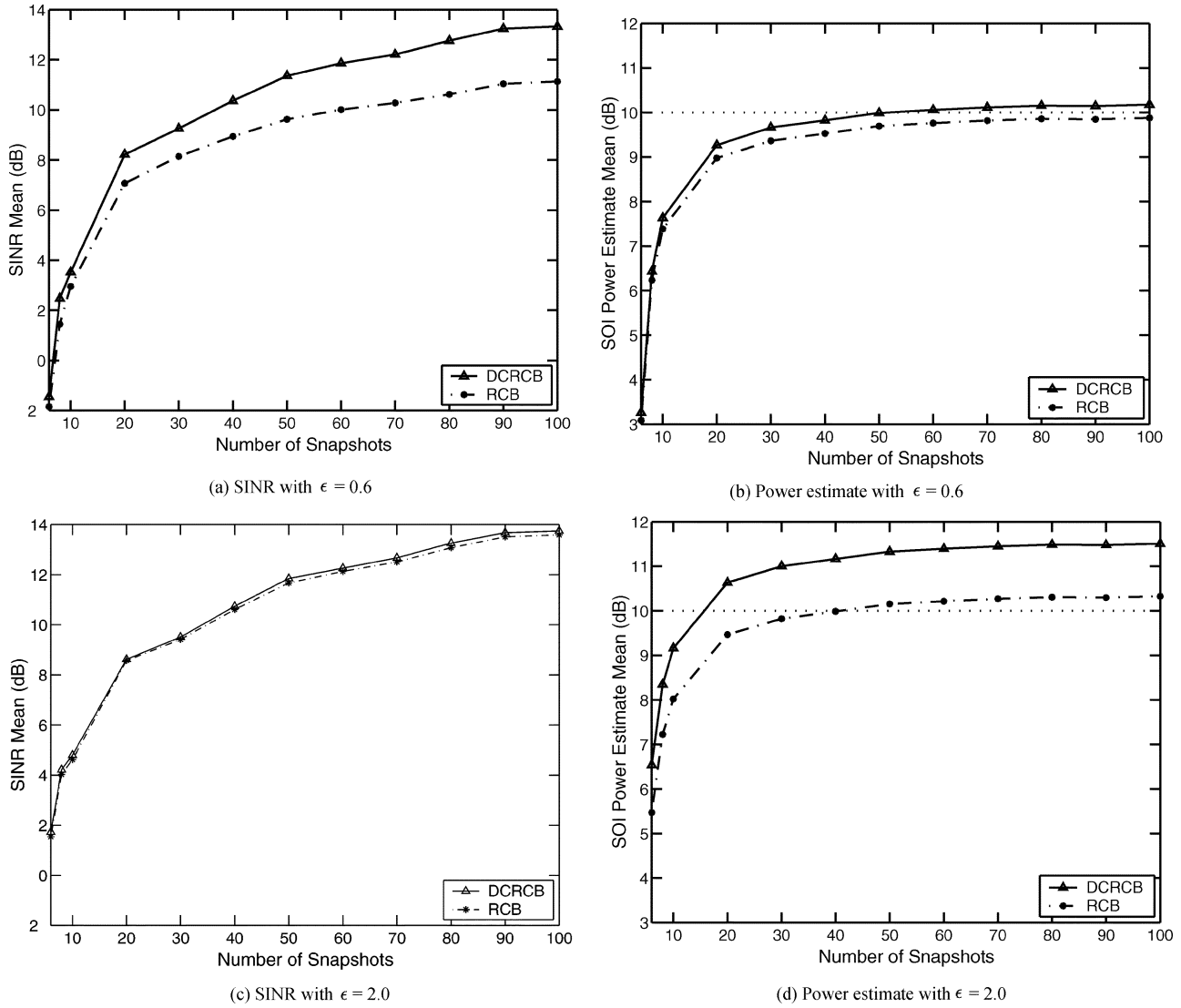


Fig. 6. Comparison of the RCB and DCRCB approaches, as the snapshot number varies, when (a), (b) $\epsilon = 0.6$ and (c), (d) $\epsilon = 2.0$. The SOI power is 10 dB, and $\epsilon_0 = 0.5603$ (corresponding to $\Delta = 2.0^\circ$).

arrival of the SOI and the other three interfering signals fixed. The array suffers from the same calibration error as in Fig. 1. Note from Fig. 5 that when the direction of arrival of an interference signal becomes too close to that of the SOI, both RCB and DCRCB suffer from severe performance degradations in both SINR and SOI power estimation accuracy. As expected, the larger the ϵ used, the weaker the interference suppression capability of both methods when an interfering signal is nearby the SOI.

We next consider the effect of the number of snapshots N on the SINR and SOI power estimation accuracy of RCB and DCRCB when the sample covariance matrix $\hat{\mathbf{R}}$ in (3) is used in lieu of the theoretical array covariance matrix \mathbf{R} . We assume that the steering vector error is due to an error in the SOI pointing angle, which we assume to be $\theta_5 + \Delta$, where θ_5 is the true arrival angle of the SOI. In this example, $\epsilon_0 = 0.5603$ corresponds to $\Delta = 2.0^\circ$. We use 100 Monte Carlo simulations to obtain the mean SINR and SOI power estimates. It is worth noting that both RCB and DCRCB allow N to be less than the number of array elements M . We use $N = 6$ and $N = 8$ for

the $N < M$ case in this example. For DCRCB, when the condition of (41) is not satisfied, we calculate the SOI power estimate by $\hat{\sigma}_0^2 = \gamma_1/M$ (as explained in Step 2 of the DCRCB algorithm). Note from Fig. 6 that the convergence properties of both methods are quite good and somewhat similar. Since the errors between $\hat{\mathbf{R}}$ and \mathbf{R} can be viewed as equivalent steering vector errors, ϵ should be chosen larger than ϵ_0 , especially for small N .

We now compare the performances of RCB and DCRCB when the power of the fourth signal is varying. As in the previous example, we have $\epsilon_0 = 0.5603$ corresponding to $\Delta = 2.0^\circ$. The INR in Fig. 7 refers to the ratio between the fourth signal power and the noise power. Note from Fig. 7(a) that the SINR of DCRCB is much better than that of RCB when $\epsilon = 0.6$. However, when ϵ is large, for example, when $\epsilon = 2.0$ as in Fig. 7(c), and when the INR is comparable to the SNR of the SOI, DCRCB has lower SINR than RCB. From the diagonal loading levels of the methods shown in Fig. 7(e) and (f), it is interesting to note that the diagonal loading level of RCB when $\epsilon = 2.0$ is about the same as that of DCRCB when $\epsilon = 0.6$.

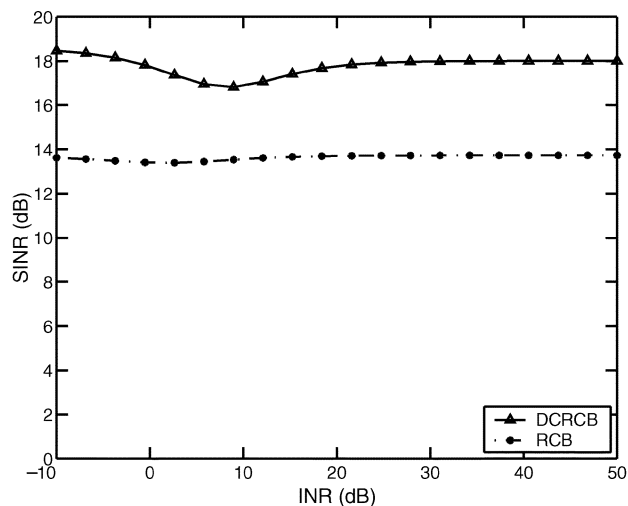
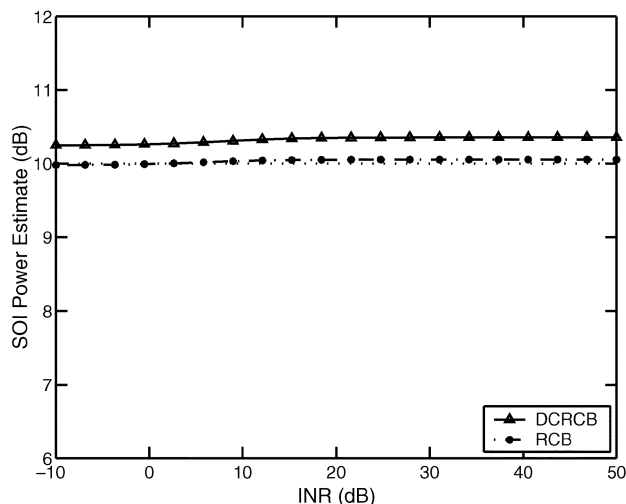
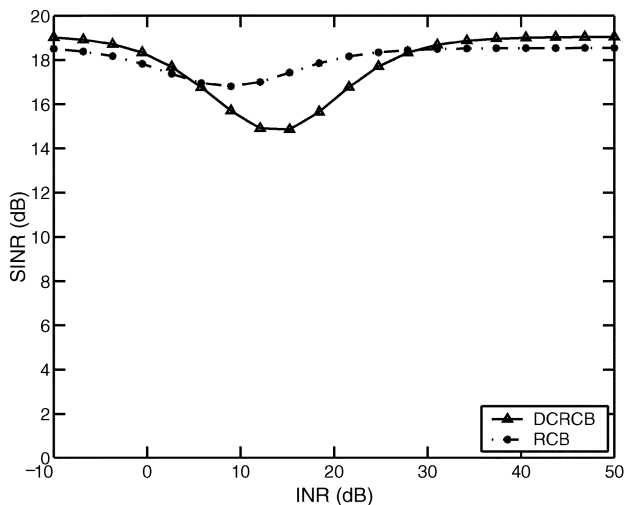
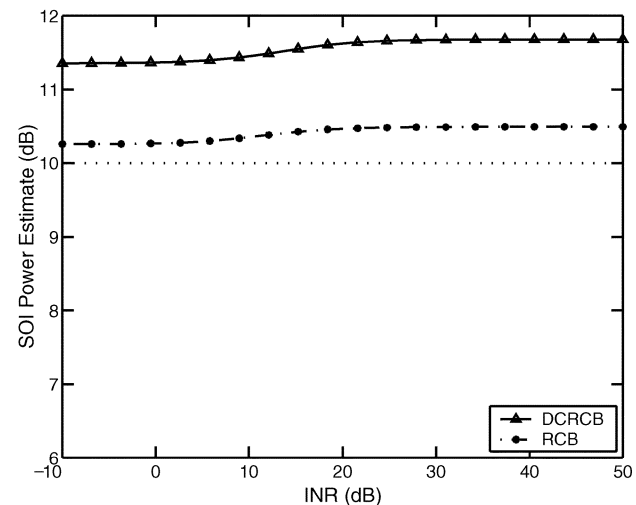
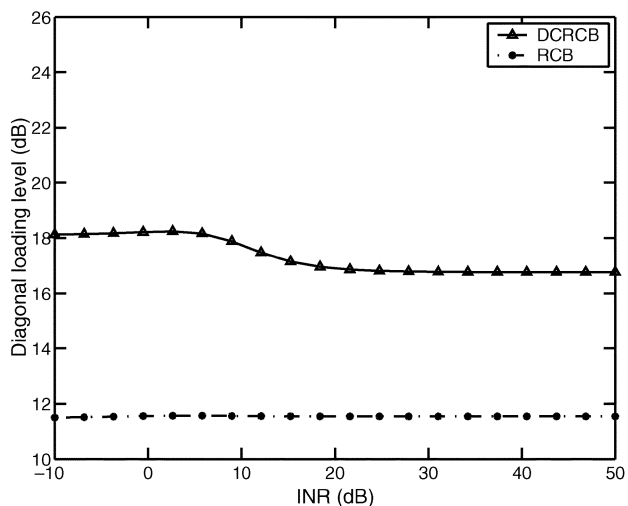
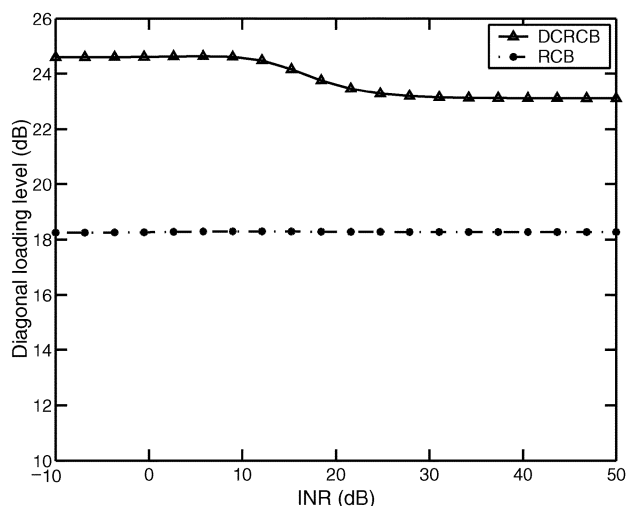
(a) SINR with $\epsilon = 0.6$ (b) Power estimate with $\epsilon = 0.6$ (c) SINR with $\epsilon = 2.0$ (d) Power estimate with $\epsilon = 2.0$ (e) Diagonal loading level for $\epsilon = 0.6$ (f) Diagonal loading level for $\epsilon = 2.0$

Fig. 7. Comparison of the RCB and DCRCB approaches with (a), (b), (e) $\epsilon = 0.6$ and (c), (d), (f) $\epsilon = 2.0$. The SOI power is 10 dB, and $\epsilon_0 = 0.5603$ (corresponding to $\Delta = 2.0^\circ$).

As a result, the SINR and SOI power estimate of RCB when $\epsilon = 2.0$ are about the same as those of DCRCB when $\epsilon = 0.6$.

Note also from Fig. 7 that when the INR becomes close to the SNR, there is a performance drop in the array output SINR. One

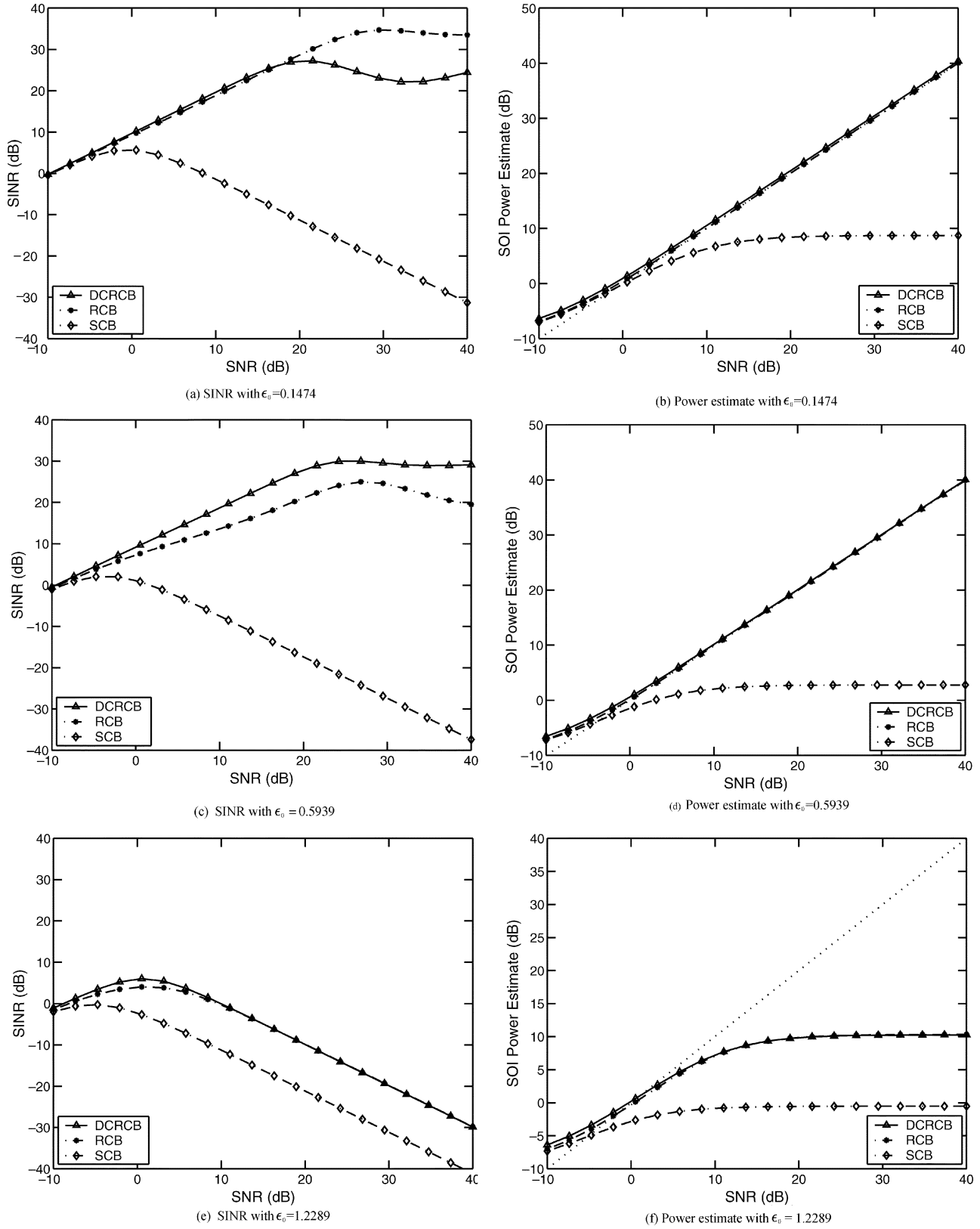


Fig. 8. Comparison of the RCB and DCRCB approaches as SNR varies when (a), (b) $\epsilon_0 = 0.1474$, (c), (d) $\epsilon_0 = 0.5939$, and (e), (f) $\epsilon_0 = 1.2289$, corresponding to $\Delta = -1.0^\circ$, -2.0° , and 3.0° , respectively. The SOI power is 10 dB, and $\epsilon = 0.6$.

possible explanation is that when the INR is much smaller than the SNR, its impact on the SOI is small. As the INR increases, it causes the SINR to drop. As the INR becomes much stronger than the SNR, the adaptive beamformers start to form deep and

accurate nulls on the interference, and as a result, the SINR improves again and then becomes stable.

Next, we consider the case where the SOI power varies. We choose $\epsilon = 0.6$ and consider three cases: $\Delta = -1.0^\circ$,

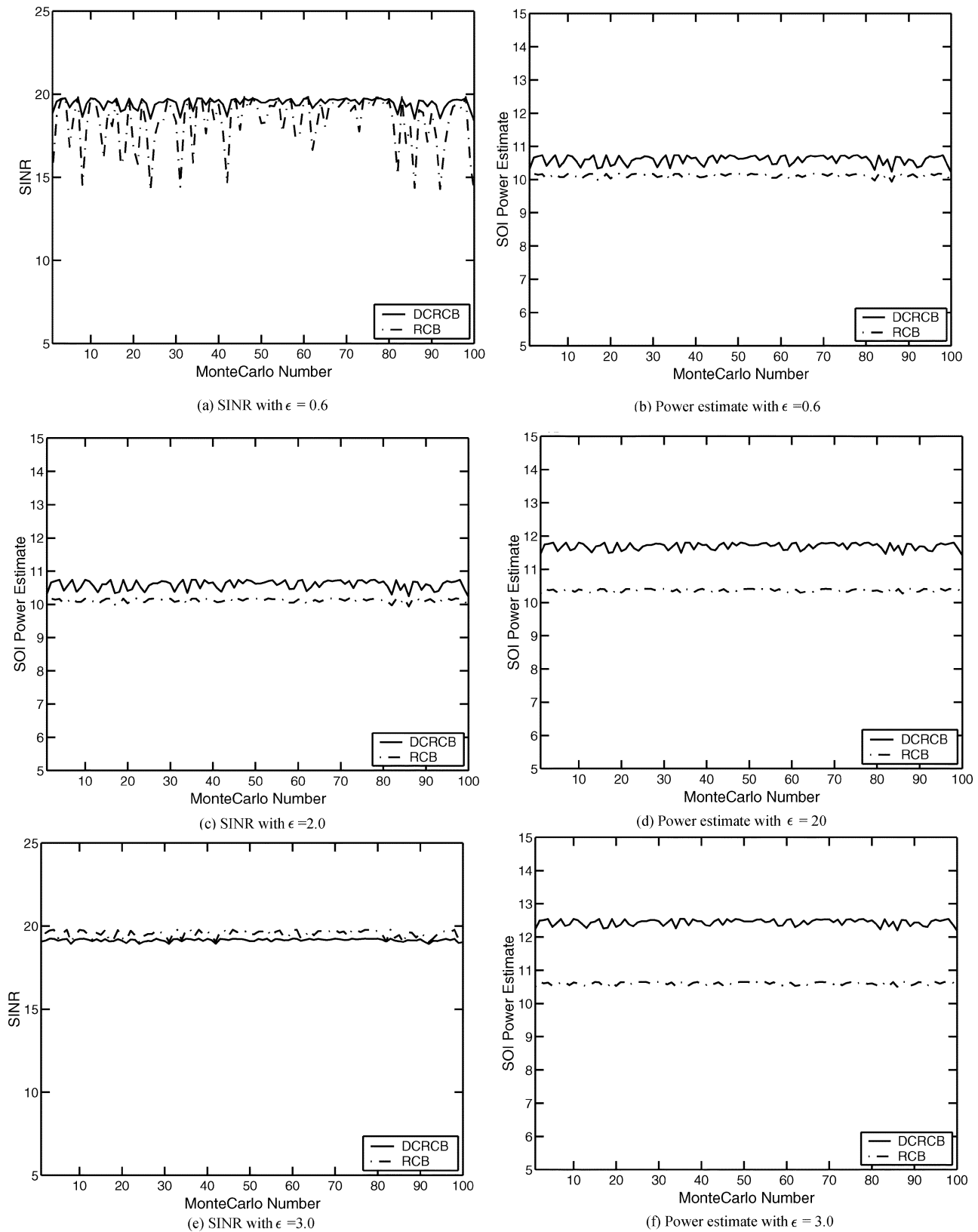


Fig. 9. Comparison of the RCB and DCRCB approaches in 100 Monte Carlo trials when (a), (b) $\epsilon = 0.6$, (c), (d) $\epsilon = 2.0$, and (e), (f) $\epsilon = 3.0$. The direction of arrival of the fifth signal is uniformly distributed between 38° and 42° , and its assumed angle is 40° . The SOI power is 10 dB, and $0 \leq \epsilon_0 \leq 0.5939$.

-2.0° , and 3.0° , with the corresponding ϵ_0 being 0.1474, 0.5939, and 1.2289, respectively. Fig. 8 shows that as long as ϵ is greater than ϵ_0 and the SOI SNR is medium or

high, the SOI power estimates of RCB and DCRCB are excellent. Their SINR curves are also quite high, but they drop when the SOI SNR approaches the INR of one of

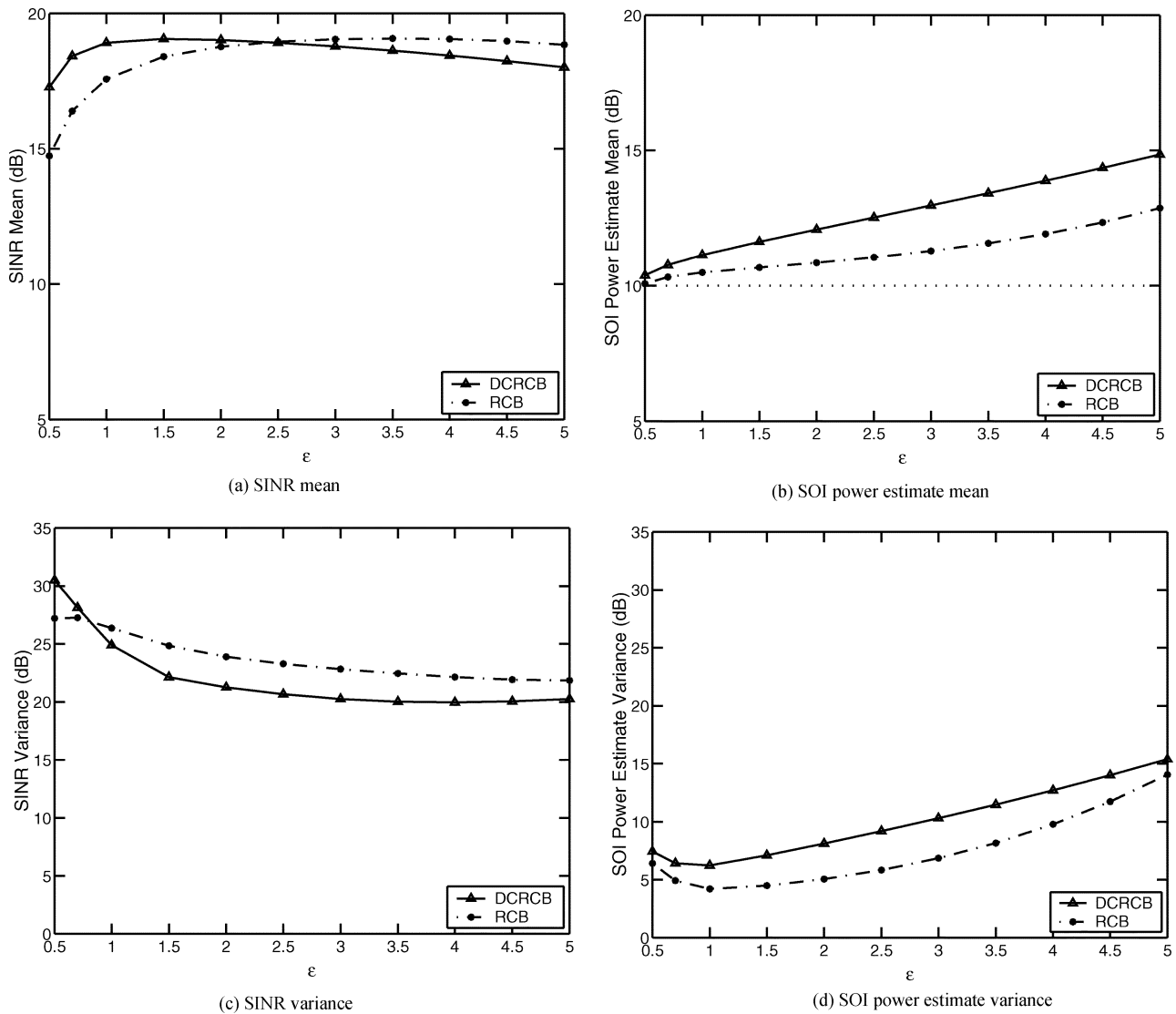


Fig. 10. Comparison of the RCB and DCRCB approaches in the presence of potentially significant array calibration errors. The SOI power is 10 dB, and $0 \leq \epsilon_0 \leq \infty$.

the interfering signals. One possible explanation is given at the end of the previous paragraph. From Fig. 8(e) and (f), we see that when ϵ is smaller than ϵ_0 , the performances of both RCB and DCRCB drop drastically as the SOI SNR increases from moderate to high. This is because the SOI is suppressed as an interference for this case. Note that RCB and DCRCB significantly outperform SCB in SINR and SOI power estimates.

Finally, in the last two examples, we use 100 Monte Carlo simulations to compare the statistical performances of RCB and DCRCB. First, the true arrival angle of the fifth signal is uniformly distributed between 38° and 42° , but it is assumed to be 40° . Fig. 9 compares the SINR and the SOI power estimates of RCB and DCRCB obtained in the 100 Monte Carlo trials. We note that the SINR mean of DCRCB is about the same as that of RCB, but the SINR variance of DCRCB is much smaller than that of RCB (especially when $\epsilon = 0.6$, which is quite tight since $0 \leq \epsilon_0 \leq 0.5939$). Hence, this example shows again that DCRCB may be preferred over RCB when higher array output SINR for waveform estimation is needed. On the other hand,

the bias and the variance of the SOI power estimates of RCB are smaller than those of DCRCB. This is especially so for large ϵ ; note that a large ϵ is not a problem here since the interfering signals are quite far away from the SOI. Hence, this example also shows that RCB may be preferred over DCRCB in applications requiring accurate SOI power estimation including radar, acoustic, and ultrasound imaging.

We next consider an example of array calibration error that consists of perturbing each element of the steering vector for each incident signal with a zero-mean circularly symmetric complex Gaussian random variable with a variance equal to 0.1. The perturbing Gaussian random variables are independent of each other. The calibration error is not scaled or normalized in any way, and hence, $0 \leq \epsilon_0 \leq \infty$. In Fig. 10, we compare the means and variances of the SINR and SOI power estimates of RCB and DCRCB, as functions of ϵ . The figure shows once again that with a reasonable choice of ϵ , DCRCB may be preferred for applications requiring high SINR, whereas RCB may be favored for applications demanding accurate SOI power estimation.

$$\begin{aligned}
h'(\lambda) &= \frac{-(\bar{\mathbf{a}}^* \mathbf{F}^{-2} 2\mathbf{F} \mathbf{F}^{-2} \bar{\mathbf{a}}) (\bar{\mathbf{a}}^* \mathbf{F}^{-1} \bar{\mathbf{a}})^2 + 2 (\bar{\mathbf{a}}^* \mathbf{F}^{-2} \bar{\mathbf{a}}) (\bar{\mathbf{a}}^* \mathbf{F}^{-1} \bar{\mathbf{a}}) (\bar{\mathbf{a}}^* \mathbf{F}^{-2} \bar{\mathbf{a}})}{(\bar{\mathbf{a}}^* \mathbf{F}^{-1} \bar{\mathbf{a}})^4} \\
&= -\frac{2 (\bar{\mathbf{a}}^* \mathbf{F}^{-1} \bar{\mathbf{a}})}{(\bar{\mathbf{a}}^* \mathbf{F}^{-1} \bar{\mathbf{a}})^4} \left[(\bar{\mathbf{a}}^* \mathbf{F}^{-3} \bar{\mathbf{a}}) (\bar{\mathbf{a}}^* \mathbf{F}^{-1} \bar{\mathbf{a}}) - (\bar{\mathbf{a}}^* \mathbf{F}^{-2} \bar{\mathbf{a}})^2 \right]. \quad (76)
\end{aligned}$$

VI. CONCLUSIONS

We have presented several ways of making the adaptive Capon beamformer robust against array steering vectors while at the same time preserving its appealing properties of high resolution and excellent interference rejection capabilities. We have shown that it is difficult to choose the norm constraint parameter in the commonly used norm-constrained Capon beamformer (NCCB) based on the knowledge of the array steering vector error alone, as such a choice should also be data-dependent. We have presented a new doubly constrained robust Capon beamformer (DCRCB), which was derived by directly addressing the steering vector uncertainty problem. We have shown that for a spherical uncertainty set of the array steering vector, the NCCB, our previous robust Capon beamformer (RCB), and our new DCRCB are all related to the diagonal loading-based approach and, in addition, that they all require a comparable computational cost with that associated with SCB. However, the diagonal loading levels of these approaches are different. As a result, RCB and DCRCB can be used to obtain much more accurate signal power estimates than NCCB under comparable conditions. We have explained the relationship between RCB and DCRCB in that the former is an approximate solution, whereas the latter is the exact solution of the same optimization problem. Our numerical examples have demonstrated that, for a reasonably tight spherical uncertainty set of the array steering vector, DCRCB is the preferred choice for applications requiring high SINR, whereas RCB is the favored one for applications demanding accurate signal power estimation.

APPENDIX ANALYSIS OF (21)

Let

$$h(\lambda) = \frac{\bar{\mathbf{a}}^* (\mathbf{R} + \lambda \mathbf{I})^{-2} \bar{\mathbf{a}}}{[\bar{\mathbf{a}}^* (\mathbf{R} + \lambda \mathbf{I})^{-1} \bar{\mathbf{a}}]^2}. \quad (72)$$

For any matrix function \mathbf{F} of λ , we have

$$(\mathbf{F}^{-1})' = -\mathbf{F}^{-1} \mathbf{F}' \mathbf{F}^{-1} \quad (73)$$

and

$$(\mathbf{F}^{-2})' = -\mathbf{F}^{-2} (\mathbf{F}' \mathbf{F} + \mathbf{F} \mathbf{F}') \mathbf{F}^{-2}. \quad (74)$$

Letting

$$\mathbf{F} = \mathbf{R} + \lambda \mathbf{I} \quad (75)$$

for which $\mathbf{F}' = \mathbf{I}$, we get (76), shown at the top of the page. For $\lambda \geq 0$, we have $\mathbf{F} > 0$. It follows that

$$\begin{aligned}
(\bar{\mathbf{a}}^* \mathbf{F}^{-2} \bar{\mathbf{a}})^2 &= (\bar{\mathbf{a}}^* \mathbf{F}^{-3/2} \mathbf{F}^{-1/2} \bar{\mathbf{a}})^2 \\
&\leq (\bar{\mathbf{a}}^* \mathbf{F}^{-3} \bar{\mathbf{a}}) (\bar{\mathbf{a}}^* \mathbf{F}^{-1} \bar{\mathbf{a}}) \quad (77)
\end{aligned}$$

and therefore, $h'(\lambda) \leq 0$ for $\lambda \geq 0$. Hence, $h(\lambda)$ is a monotonically decreasing function of $\lambda \geq 0$. As $\lambda \rightarrow \infty$, $h(\lambda) \rightarrow 1/M < \zeta$, according to (26). From (14), $h(0) > \zeta$ since $h(0)$ is equal to the right side of (14). This shows that, indeed, (21) has a unique solution $\lambda > 0$ under (14) and (26).

REFERENCES

- [1] P. Stoica and R. L. Moses, *Introduction to Spectral Analysis*. Englewood Cliffs, NJ: Prentice-Hall, 1997.
- [2] H. L. Van Trees, *Detection, Estimation, and Modulation Theory, Part IV, Optimum Array Processing*. New York: Wiley, 2002.
- [3] J. Capon, "High resolution frequency-wavenumber spectrum analysis," *Proc. IEEE*, vol. 57, pp. 1408–1418, Aug. 1969.
- [4] R. T. Lacoss, "Data adaptive spectral analysis methods," *Geophys.*, vol. 36, no. 4, pp. 661–675, Aug. 1971.
- [5] C. D. Seligson, "Comments on high resolution frequency-wavenumber spectrum analysis," *Proc. IEEE*, vol. 58, pp. 947–949, 1970.
- [6] H. Cox, "Resolving power and sensitivity to mismatch of optimum array processors," *J. Acoust. Soc. Amer.*, vol. 54, no. 3, pp. 771–785, 1973.
- [7] D. D. Feldman and L. J. Griffiths, "A projection approach for robust adaptive beamforming," *IEEE Trans. Signal Processing*, vol. 42, pp. 867–876, Apr. 1994.
- [8] A. K. Steele, "Comparison of directional and derivative constraints for beamformers subject to multiple linear constraints," *Proc. Inst. Elect. Eng. F, H*, vol. 130, no. 1, pp. 41–45, Feb. 1983.
- [9] A. B. Gershman, "Robust adaptive beamforming in sensor arrays," *Int. J. Electron. Commun.*, vol. 53, no. 6, pp. 305–314, 1999.
- [10] S. A. Vorobyov, A. B. Gershman, and Z.-Q. Luo, "Robust adaptive beamforming using worst-case performance optimization: A solution to the signal mismatch problem," *IEEE Trans. Signal Processing*, vol. 51, pp. 313–324, Feb. 2003.
- [11] R. G. Lorenz and S. P. Boyd, "Robust minimum variance beamforming," *IEEE Trans. Signal Processing*, 2001, submitted for publication.
- [12] J. Li, P. Stoica, and Z. Wang, "On robust Capon beamforming and diagonal loading," *IEEE Trans. Signal Processing*, vol. 51, pp. 1702–1715, July 2003.
- [13] J. E. Hudson, *Adaptive Array Principles*. London, U.K.: Peter Peregrinus, 1981.
- [14] Y. I. Abramovich and A. I. Nevrev, "An analysis of effectiveness of adaptive maximization of the signal-to-noise ratio which utilizes the inversion of the estimated correlation matrix," *Radio Eng. Electron. Phys.*, vol. 26, pp. 67–74, Dec. 1981.
- [15] M. H. Er and A. Cantoni, "An alternative formulation for an optimum beamformer with robustness capability," *Proc. Int. Elect. Eng. F, Commun., Radar, Signal Process.*, vol. 132, pp. 447–460, 1985.
- [16] H. Cox, R. M. Zeskind, and M. M. Owen, "Robust adaptive beamforming," *IEEE Trans. Acoust., Speech, Signal Processing*, vol. ASSP-35, pp. 1365–1376, Oct. 1987.
- [17] B. D. Carlson, "Covariance matrix estimation errors and diagonal loading in adaptive arrays," *IEEE Trans. Aerosp. Electron. Syst.*, vol. 24, pp. 397–401, July 1988.
- [18] Y. I. Abramovich, V. G. Kachur, and V. N. Mikhaylyukov, "The convergence of directivity and its stabilization in fast spatial filter adaptive tuning procedures," *Soviet J. Commun. Technol. Electron.*, vol. 34, no. 15, pp. 6–11, 1989.
- [19] Y. I. Abramovich and V. G. Kachur, "Methods of protecting a useful signal differing from reference in adaptive procedures with unclassified teaching sample," *Soviet J. Commun. Technol. Electron.*, vol. 35, no. 13, pp. 29–35, 1990.
- [20] B. D. Van Veen, "Minimum variance beamforming with soft response constraints," *IEEE Trans. Signal Processing*, vol. 39, pp. 1964–1972, Sept. 1991.
- [21] R. Wu, Z. Bao, and Y. Ma, "Control of peak sidelobe level in adaptive arrays," *IEEE Trans. Antennas Propagat.*, vol. 44, pp. 1341–1347, Oct. 1996.

- [22] C.-C. Lee and J.-H. Lee, "Robust adaptive array beamforming under steering vector errors," *IEEE Trans. Antennas Propagat.*, vol. 45, pp. 168–175, Jan. 1997.
- [23] Z. Tian, K. L. Bell, and H. L. Van Trees, "A recursive least squares implementation for LCMP beamforming under quadratic constraints," *IEEE Trans. Signal Processing*, vol. 49, pp. 1138–1145, June 2001.
- [24] S. Q. Wu and J. Y. Zhang, "New robust beamforming method with antennae calibration errors," in *Proc. IEEE Wireless Commun. Networking Conf.*, vol. 2, New Orleans, LA, Sept. 1999, pp. 869–872.
- [25] P. Stoica, Z. Wang, and J. Li, "Robust Capon beamforming," *IEEE Signal Processing Lett.*, vol. 10, pp. 172–175, June 2003.
- [26] S. Shahbazpanahi, A. B. Gershman, Z.-Q. Luo, and K. M. Wong, "Robust adaptive beamforming using worst-case SINR optimization: A new diagonal loading-type solution for general-rank signal models," *Proc. ICASSP*, vol. 5, no. 1, pp. 333–336, Apr. 2003.
- [27] T. L. Marzetta, "A new interpretation for Capon's maximum likelihood method of frequency-wavenumber spectrum estimation," *IEEE Trans. Acoust., Speech, Signal Processing*, vol. ASSP-31, pp. 445–449, Apr. 1983.
- [28] C. A. Stutt and L. J. Spafford, "A best mismatched filter response for radar clutter discrimination," *IEEE Trans. Inform. Theory*, vol. IT-14, pp. 280–287, Mar. 1968.



Jian Li (S'87–M'91–SM'97) received the M.Sc. and Ph.D. degrees in electrical engineering from The Ohio State University (OSU), Columbus, in 1987 and 1991, respectively.

From April 1991 to June 1991, she was an Adjunct Assistant Professor with the Department of Electrical Engineering, OSU. From July 1991 to June 1993, she was an Assistant Professor with the Department of Electrical Engineering, University of Kentucky, Lexington. Since August 1993, she has been with the Department of Electrical and

Computer Engineering, University of Florida, Gainesville, where she is currently a Professor. Her current research interests include spectral estimation, array signal processing, and their applications.

Dr. Li is a member of Sigma Xi and Phi Kappa Phi. She received the 1994 National Science Foundation Young Investigator Award and the 1996 Office of Naval Research Young Investigator Award. She was an Executive Committee Member of the 2002 International Conference on Acoustics, Speech, and Signal Processing, Orlando, FL, May 2002. She has been an Associate Editor of the *IEEE TRANSACTIONS ON SIGNAL PROCESSING* since 1999. She is presently a member of the Signal Processing Theory and Methods (SPTM) Technical Committee of the IEEE Signal Processing Society.

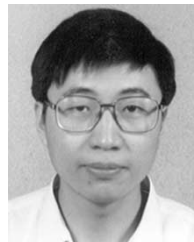


Petre Stoica (F'94) received the D.Sc. degree in automatic control from the Polytechnic Institute of Bucharest (BPI), Bucharest, Romania, in 1979 and an honorary doctorate degree in science from Uppsala University (UU), Uppsala, Sweden, in 1993.

He is Professor of system modeling with the Department of Systems and Control at UU. Previously, he was a Professor of system identification and signal processing with the Faculty of Automatic Control and Computers at BPI. He held longer visiting positions with Eindhoven University of Technology, Eindhoven, The Netherlands;

Chalmers University of Technology, Gothenburg, Sweden (where he held a Jubilee Visiting Professorship); UU; The University of Florida, Gainesville; and Stanford University, Stanford, CA. His main scientific interests are in the areas of system identification, time series analysis and prediction, statistical signal and array processing, spectral analysis, wireless communications, and radar signal processing. He has published seven books, ten book chapters, and some 500 papers in archival journals and conference records on these topics. The most recent book he co-authored, with R. Moses, is entitled *Introduction to Spectral Analysis* (Englewood Cliffs, NJ: Prentice-Hall, 1997). Recently, he edited two books on signal processing advances in wireless communications and mobile communications (Englewood Cliffs, NJ: Prentice-Hall, 2001). He is on the editorial boards of five journals in the field: *Journal of Forecasting*; *Signal Processing*; *Circuits, Signals, and Signal Processing*; *Digital Signal Processing—A Review Journal*; and *Multidimensional Systems and Signal Processing*. He was a Co-Guest Editor for several special issues on system identification, signal processing, spectral analysis, and radar for some of the aforementioned journals, as well as for *PROCEEDINGS OF THE IEEE*.

Dr. Stoica was co-recipient of the IEEE ASSP Senior Award for a paper on statistical aspects of array signal processing. He was also recipient of the Technical Achievement Award of the IEEE Signal Processing Society for fundamental contributions to statistical signal processing with applications in time-series analysis, system identification, and array signal processing. In 1998, he was the recipient of a Senior Individual Grant Award of the Swedish Foundation for Strategic Research. He was also co-recipient of the 1998 EURASIP Best Paper Award for Signal Processing for a work on parameter estimation of exponential signals with time-varying amplitude, a 1999 IEEE Signal Processing Society Best Paper Award for a paper on parameter and rank estimation of reduced-rank regression, a 2000 IEEE Third Millennium Medal, and the 2000 W. R. G. Baker Prize Paper Award for a paper on maximum likelihood methods for radar. He was a member of the international program committees of many topical conferences. From 1981 to 1986, he was the Director of the International Time-Series Analysis and Forecasting Society, and he has been a member of the IFAC Technical Committee on Modeling, Identification, and Signal Processing since 1994. He is also a member of the Romanian Academy and a Fellow of the Royal Statistical Society.



Zhisong Wang (S'02) received the B.E. degree in electrical engineering from Tongji University, Shanghai, China, in 1998. Since May 2001, he has been a research assistant with the Department of Electrical and Computer Engineering, the University of Florida, Gainesville, where he is pursuing the Ph.D. degree in electrical engineering.

His current research interests include spectral estimation, array signal processing, optimization, and signal processing for acoustic and radar applications.